

# **Effect of artificial drought stress on sap flow of different tree species in the eastern Himalaya**

**Masterarbeit** zur Erlangung des DI  
an der Universität für Bodenkultur

eingereicht von:

Josef **Gadermaier**

(Matrikelnr.: 0540446)

Semester: WS 2017

Supervisors:

Univ.-Prof. Mag. Dr. **Peter Hietz**

Ao. Univ.Prof. Dipl.-Ing. Dr. **Georg Gratzer**

## **Eidesstattliche Erklärung**

Hiermit erkläre ich, dass die vorliegende Masterarbeit selbstständig von mir verfasst wurde. Es wurden keine weiteren Quellen verwendet bis auf die im Literaturverzeichnis angeführten. Diese wurden wörtlich und inhaltlich übernommen und als solche gekennzeichnet. Wörtlich oder sinngemäß übernommenes Gedankengut habe ich als solches kenntlich gemacht.

Ort, Datum

Unterschrift

## Kurzfassung

Dendrochronologische Untersuchungen haben gezeigt, dass es in den letzten 500 Jahren aufgrund von weltweit erhöhten Temperaturen zu Abschwächungen und Ausfällen des Monsuns kam. Durch die aktuelle globale Temperaturerhöhung wird vermutet, dass es in Zukunft zu ähnlichen extremen Dürreereignissen kommen kann. Zur Simulation einer solchen Dürre wurden im Jahr 2014 in zwei Bergwaldtypen in Bhutan insgesamt vier Dächer in zwei Meter Höhe mit einer Gesamtfläche von 2.400 m<sup>2</sup> errichtet und ein umfangreiches Mess-System installiert. In dieser Arbeit werden die Daten der installierten Saftstromsensoren von insgesamt 60 Bäumen, aufgeteilt auf fünf Baumarten, untersucht. Die Baumarten beinhalten eine Nadelbaumart (*Tsuga dumosa*), drei Eichenarten mit unterschiedlichen Eigenschaften (*Quercus griffithii* – laubabwerfend, *Quercus semecarpifolia* und *Quercus lanata* – immergrün) und eine Rhododendrenart im Unterwuchs (*Rhododendron arboreum*). Mit Hilfe der Saftstromdaten und unter Einbezug von Bodenfeuchte- und Klimadaten von montierten Wetterstationen, wurden die unterschiedlichen Reaktionen der untersuchten Baumarten auf die simulierte Dürre dargestellt. In zwei Baumarten (*Rhododendron arboreum*, *Quercus lanata*), konnte während des Beobachtungszeitraums (drei Monate im Jahr 2016) kein Unterschied zwischen den Bäumen unter den Dächern und Bäumen auf den Kontrollflächen gemessen werden. Die restlichen Baumarten zeigten während der Monsun-Zeit meist geringe Unterschiede. Dieser Unterschied war allerdings in der folgenden Trockenzeit mit höherem Dampfdruckdefizit der Luft stärker ausgeprägt. Die Zeitverzögerung zwischen den treibenden Klimaparametern und Saftfluss war bei *Tsuga dumosa* am höchsten, was auf eine relativ hohe Wasserspeicherkapazität des Stammes hinweist. Um genauere Aussagen über die Trockenresistenz der Bäume treffen zu können sollten längere Messzeiträume und weitere Daten über die untersuchten Baumarten erhoben und ausgewertet werden.

## Abstract

Ongoing climate change may result in more frequent monsoon failures in the future. This would cause severe droughts in the affected areas and lead to changes in the ecosystems. To simulate such a drought, four through-fall exclusion plots, covering a total area of 2.400 m<sup>2</sup>, were established in two main Bhutanese forest types in 2014 and compared with control plots receiving normal rainfall. Additionally, climate and soil water were monitored. In this study, data from sap flow sensors on 60 trees from five tree species are evaluated. The five tree species include one conifer (*Tsuga dumosa*) three oak species differing in phenology (*Quercus griffithii* – deciduous, *Quercus lanata* and *Quercus semecarpifolia* – evergreen) and one *Rhododendron* species in the understorey (*Rhododendron arboreum*). The analysis of sap flow data with soil moisture and climate from the different sites and plots shows the different reactions of tree species to the simulated drought. During the measurement period (three months in 2016), two species (*Rhododendron arboreum* and *Quercus lanata*) showed no differences between trees on the control plots and the through-fall exclusion plots. During the monsoon season, in the other species the drought-stressed trees had significantly lower sap flow. In the following dry period, with higher vapour pressure deficit of the, this difference increased. The time-lag between the driving climate parameters and sap flow was greatest in *Tsuga dumosa*, suggesting that this species has a relatively high stem water storage capacitance. For a better understanding of the resilience to drought of the species studied, in the future longer sap flow time series should be analysed together with additional data of the trees.

# Table of content

1	Introduction .....	10
1.1	Global warming and the Himalayan region.....	10
1.2	Water and plants .....	11
1.2.1	Water transport in plants.....	11
1.2.2	Drivers of transpiration .....	13
1.2.3	Water storage capacity of trees.....	14
1.2.4	Drought stress in trees.....	14
1.3	Simulating drought stress conditions on forest ecosystems in the Himalaya region.....	15
1.3.1	The through-fall exclusion experiment.....	16
1.3.2	Sap flow and drought stress.....	16
1.4	Goals and hypothesis of through-fall exclusion experiment.....	17
2	Material and methods .....	19
2.1	The study sites.....	19
2.2	Climate and weather.....	20
2.3	Soil characteristics.....	22
2.4	Examined tree species.....	23
2.5	The through-fall exclusion experiment.....	25
2.5.1	The through-fall exclusion roofs.....	25
2.5.2	Sap flow measurements .....	27
2.6	Data analysis and corrections .....	34
2.6.1	Correction of sap flow signals.....	34
2.6.2	Calculation of sap flow density ( $Q_s$ ).....	37
2.6.3	Calculation of normalised $Q_s$ ( $Q_{s-sum}$ ) .....	39
2.6.4	Calculation of sap flow time lag.....	40
2.6.5	Applied statistical methods .....	40
3	Results .....	41
3.1	Soil water content .....	41
3.2	Weather data.....	42
3.3	Sap flow data .....	45
3.3.1	Correlation of $Q_{s-nor}$ with environmental factors .....	48
3.3.2	Linear regression models for sap flow and environmental factors .....	52

3.3.3	Time lag of $Q_s$ and environmental factors .....	54
4	Discussion & Conclusion.....	60
4.1	Experimental design.....	60
4.2	Impact of through-fall exclusion roofs on sap flow density.....	60
4.3	Impact of main environmental drivers on sap flow.....	61
4.4	Time lags .....	63
4.5	Sap flow and drought stress susceptibility.....	64
4.6	Conclusions and Outlook.....	65
5	Literature .....	67

## List of Tables

Table 1: A list of through-fall experiments in wet tropical or subtropical regions (Bonal et al., 2016). .....	16
Table 2: Characteristics of experimental plots.....	20
Table 3: Soil profiles and soil horizon description for both forest types (Wangdi, 2016).....	22
Table 4: Distribution of SWC <sub>v</sub> sensors in the soil profiles at all plots.....	23
Table 5: Number of individuals per species and site included in the study.....	27
Table 6: List of trees with sap flow sensors (Wangdi, 2016).....	28
Table 7: Pearson correlation coefficients and significance levels for climatic variables and standardized sap flow density separated by treatment (control/roof). .....	48
Table 8: p-values of ANCOVA-test for treatment effect in correlation of Q <sub>s-nor</sub> and D.....	49
Table 9: : p-values of ANCOVA-test for treatment effect in correlation of Q <sub>s-nor</sub> and E.....	51
Table 10: Estimates and R <sup>2</sup> values from linear regression for climatic variables and Q <sub>s-nor</sub> separated by treatment (control/roof). .....	53
Table 11: Statistical summary for ANOVA-analysis testing the differences in lags (from D) by treatment. ....	55
Table 12: Statistical summary for ANOVA-analysis testing the differences in lags (from E) by treatment.	58

## List of Figures

Figure 1: Tracheids and vessel elements (simplified) (Taiz et al., 2002).....	12
Figure 2: Location of the through-fall exclusion experiment in Bhutan (TG = Tashigang Goempa, PG = Pangsho Goempa). (Om, 2016).....	19
Figure 3: Walter`s climate diagram for representative sites along altitudinal gradient (Dochula - mixed coniferous forest, Lumitsawa - broadleaf forest, modified). ....	20
Figure 4: Monthly mean maximum air temperature [°C], Minimum air temperature [°C] and total precipitation [mm * M <sup>-1</sup> ] at the mixed coniferous forest site (a) and the broadleaf forest site (b).....	21
Figure 5: Mixed coniferous forest site in Bhutan/Thimphu district. ....	24
Figure 6: Broadleaf forest site, Bhutan/Wangdue Phodrang district. ....	24
Figure 7: Wooden structure without plastic foil at the broadleaf forest site, Bhutan/Wangdue Phodrang district. ....	25
Figure 8: Roof with plastic foil at the broadleaf forest site, Bhutan/Wangdue Phodrang district. ....	26
Figure 9: Roof at the mixed coniferous site, Bhutan/Thimphu district. ....	26
Figure 10: Trenches at roof plots to avoid water flow from upslope.....	27
Figure 11: Schematic overview of Granier system for sap flow measurements. (Lu et al., 2004) .....	29
Figure 12: Temperature difference between heated and unheated probe as a function of sap flow velocity.....	30
Figure 13: Schematic overview of the measurement setup at every plot. ....	30
Figure 14: Close-up of applied Granier-type sap flow sensor and drillers for perforating tree stems.....	31
Figure 15: Radial patterns of relative active sapwood in different tree species, 100 represents the layer immediately beneath the cambium (a = <i>Pinus sylvestris</i> , b = <i>Populus hybrid</i> , c = <i>Quercus petraea</i> , d = <i>Olea europea</i> , e = <i>Ficus carica</i> , f = <i>Shorea sumatrana</i> ). ....	33
Figure 16: Mounting procedure of sap flow sensors during field work. a) tree stem with removed bark; b) mounted sap flow sensors without cover; c) mounted sensors with insulation. ....	34
Figure 17: Simple correction of sensor signal according to input voltage. ....	35
Figure 18: Comparison of 04:00 AM values for sensor 57O during blackout.....	36
Figure 19: Corrected mV-signals for sensor 57O after implementation of second correction factor. ....	37
Figure 20: Calculated $Q_s$ of trees at the broadleaf forest site (Pangsho Goempa = PG) separated by treatment and in comparison to D and E.....	38
Figure 21: Calculated sap flow density of trees at the mixed conifer forest site (Tashigang Goempa = TG) separated by treatment and in comparison to D and E. ....	39
Figure 22: Mean volumetric water content per plot in Pangsho Goempa (broadleaf forest - left) and for Tashigang Goempa (mixed conifer forest – right) for measurements until 50 cm depth from May until November 2016.41	



Figure 23: Mean volumetric water content per plot in Pangsho Goempa (PG, broadleaf forest - left) and for Tashigang Goempa (TG, mixed conifer forest – right) for measurements until 50 cm depth during the measurement period.....	41
Figure 24: Mean volumetric water content per site and treatment in relationship to precipitation (Tashigang Goempa - right, Pangsho Goempa - left).....	42
Figure 25: Climate data at the broadleaf forest (PG) and mixed conifer forest (TG). ....	43
Figure 26: Correlation matrix of daily means/sums of climatic variables at Tashigang Goempa (mixed coniferous forest).....	44
Figure 27: Correlation matrix of daily means/sums of climatic variables at Pangsho Goempa (broadleaf forest). .....	44
Figure 28: Mean daily sap flow density per species and treatment. The shaded grey areas represent the standard deviation within the species (dark grey = SD control, bright grey = SD treatment).....	46
Figure 29: Comparison of p-values from t-test to evaluate differences between control and roof plots over time (the grey line represents the 0.05 significance level). ....	46
Figure 30: Mean daily sap flow density per species and treatment. The shaded grey areas are representing the standard error within the species (dark grey = SE control, bright grey = SE treatment). ....	47
Figure 31: Sap flow density of single trees for <i>Quercus lanata</i> on six days in November 2016. ....	48
Figure 32: Correlation of $Q_{s-nor}$ (=relative sap flow density) and D per tree species.....	50
Figure 33: Correlation of $Q_{s-nor}$ (=relative sap flow density) and E per tree species. ....	51
Figure 34: Correlation of $Q_{s-nor}$ (=relative sap flow density) and SWCv per tree species.....	52
Figure 35: Time lags of $Q_s$ to D of different tree species distinguished by treatment.....	54
Figure 36: Diurnal pattern of $Q_s$ and D for a day in November 2016.....	55
Figure 37: Diurnal shape of $Q_s$ in % of the daily maximum value for the whole measurement period in comparison to D for <i>Tsuga dumosa</i> . ....	56
Figure 38: Diurnal shape of $Q_s$ in % of the daily maximum value for the whole measurement period in comparison to D for <i>Quercus lanata</i> .....	56
Figure 39: Comparison of mean diurnal course of vapour pressure deficit and irradiance for both sites (in % of daily maximum).....	57
Figure 40: Time lags of $Q_s$ to E for different tree species distinguished by treatment. ....	58
Figure 41: Diurnal shape of sap flow density in % of the daily maximum value for the whole measurement period in comparison to E for <i>Tsuga dumosa</i> .....	59
Figure 42: Diurnal shape of $Q_s$ in % of the daily maximum value for the whole measurement period in comparison to E for <i>Quercus lanata</i> . ....	59

# 1 Introduction

## 1.1 Global warming and the Himalayan region

It is projected that with higher temperatures and altered climatic systems, tree mortality and forest dieback will be increasing. This trend can have negative consequences as the forests cannot entirely fulfill their ecosystem services anymore. It is also projected that substantial carbon losses might occur through the degradation of forest ecosystems causing a further increase of the CO<sub>2</sub> concentration in the atmosphere (IPCC, 2014). Changes in terrestrial ecosystems can also contribute to a changing climate as they are the source of transpiration, a main driver in the climate system of the earth. Globally, it accounts for 61% of evapotranspiration on the terrestrial surface, and 39% of rainfall is transpired back to the atmosphere. It is expected that changes in transpiration through increasing CO<sub>2</sub> concentrations, land use changes, shifting ecozones and climate warming are having significant impacts upon runoff and groundwater recharge. (Schlesinger et al., 2014).

The Greater Himalayan region, covering approximately seven million km<sup>2</sup>, is a key element in the climate system of Asia and a main factor for the summer monsoon in this area. Because of its geographic and biological diversity, the area is considered to be one of the biodiversity hotspots of the planet (Xu et al., 2009).

New studies state that with higher altitude, the rate of warming is increased (Pepin et al., 2015). Therefore, high-mountain environments like the Himalayan region may undergo more rapid changes than lowland environments. For example the temperature increase on the Tibetan Plateau has been more than two times the global average (Xu et al., 2014). This rise in temperature is mostly visible in the melting of the glaciers in the area, but it also will strongly affect the ecosystems and the climatic system as a whole (Xu et al., 2009).

One of the most important climatic factors for the ecosystems in the Southern Himalaya is the Indian summer monsoon from June to September. It accounts for the main annual rainfalls in most of the regions south of the main ridge of the Himalayas, where Bhutan is also located. Precipitation in Bhutan depends on the elevation, and the complex topographic variations within the Inner Himalayan region. The high mountains in the south of the country act as orographic borders, causing high annual precipitation for this area up to 5500 mm/a. Precipitation decreases towards the north depending on the topography, to <400 mm/a in the high altitude mountains at the northern border (Khandu et al., 2016).

Records of monsoon failures in the last millennium are well documented in the MADA (Monsoon, Asia Drought Atlas) developed by Cook et al. (2010). This spatial tool for monsoon failures identified droughts via tree ring analysis in the whole area affected by Asia's monsoon. The base for the study are more than 300 sites for tree ring analysis including Bhutan. Although mega droughts occurred in the past, the data in the MADA did not show a high frequency of these events. The authors mainly identify four megadroughts in the last 500 years. However, statistically predictive models for future monsoon failures in India are predicting a more frequent occurrence of monsoon failures and drought periods in the region. This is mainly

caused by increased temperatures due to global warming especially in water temperatures in the Pacific Ocean (Schewe & Levermann, 2012; Menon et al., 2013).

Located in the eastern Himalayas, 71% of Bhutan's territory is covered with forests (MoAF, 2017). Therefore, the ecosystem services provided by the forest are of high importance for the country. Fast changes in the forests caused by climate change or droughts can have severe negative effects causing limited provision of these services (N. McDowell et al., 2008).

One example of effects of droughts in forests related to the climatic system is the declined evaporative cooling effect of forests if droughts appear to happen more frequently (Bonan, 2008). On a forest level, tree mortality is likely to increase. Trees often experience water stress as a trigger, mostly in combination with other biotic agents like wood-boring insects or fungal pathogens that finally cause the death of the plant (Allen et al., 2010). Through tree mortality, changing temperatures, altered precipitation patterns and further changes in the ecosystem caused by a changing climate, forests can experience large-scale shifts in their structure and function (N. McDowell et al., 2008).

Partial monsoon failures would lead to lower water availability and to drought stress for the ecosystems. Full monsoon failures will lead to severe drought stress for forest ecosystems for one year or even several years if monsoon does not occur for longer. Plants possess different strategies to deal with drought stress, such as regulating water use. As this study is mostly focusing on the water transport in trees during drought stress, the following chapters describe the most important processes in trees related to water.

## **1.2 Water and plants**

Besides oxygen (O<sub>2</sub>) and carbon dioxide (CO<sub>2</sub>), which are available from the atmosphere, plants require at least 15 additional elements. These elements have to be taken up as dissolved anorganic nutrients in water. Therefore, water uptake, transport and storage are crucial functions to ensure plant growth and survival (Brennicke et al., 2010).

### **1.2.1 Water transport in plants**

Water uptake starts (besides a few exceptions of water uptake of plant parts directly from the atmosphere) at the root's surface. There are three possible ways for radial water transport into the roots central cylinder. The apoplastic pathway leads towards the extracellular space where the water can diffuse freely until it is interrupted by the Casparian strip. The symplastic pathway is slower and leads within the cytoplasm towards the central cylinder of the plant (Pott & Hüppe, 2007, p. 237). The third pathway is the transcellular transport, where the water crosses directly via the cells and has to pass through several cell membranes (Schopfer et al., 2010, p.314).

Finally, water and selected nutrients enter the far distance transport system of the plant via passage cells. These cells are located close to the xylem in vascular bundles which regulate the flow towards the xylem. Due to its di-polarity, water forms hydrogen bridges, which cause high cohesion forces. Together with adhesion forces, it enables the capillary transport of water in the xylem (Schopfer et al., 2010, p. 298).

There exist different types of vascular bundles depending on the plant type as well as where the vascular bundle is located (root, leaf, shoot axis). A main distinction between vascular bundle types can be made between concentric, radial, collateral- and bi-collateral vascular bundles (Tobergte & Curtis, 2013, p. 50). As this thesis only deals with the water transport in tree species, only these types of vascular bundles will be outlined.

The structure and system of the xylem is particularly important, as in most plants water is transported almost exclusively through the xylem. In a plant 1 m tall, around 99.5 % of the total water pathway is through the xylem and in tall growing trees this share is even higher (Taiz & Zeiger, 2010, p. 52).

### 1.2.1.1 Xylem structure in coniferous trees

In gymnosperms, tracheids are formed for the water transport in the plant. These tubular structures are elongated, spindle-shaped cells which are arranged in overlapping vertical files (Figure 1). Tracheids, as well as vessel cells, are large, elongated dead cells without any organelles or membranes and thick lignified cell walls. Water can move between the tracheids via pits laterally positioned on the cell walls. Water flows through this pits and rises further in the next tracheid cell (Taiz & Zeiger, 2010, p. 53).

In comparison to angiosperms, the wood of gymnosperms shows a simpler structure and mainly consists of tracheids and thin parenchymatous radial rays. The early-wood tracheids, formed in spring during the main growth period, have thin cell walls and a larger diameter. Later in summer cell walls are thicker and the lumen of the tracheids decreases. Also typical for gymnosperms are transversal tracheids responsible for radial transport (Tobergte & Curtis, 2013, p. 64).

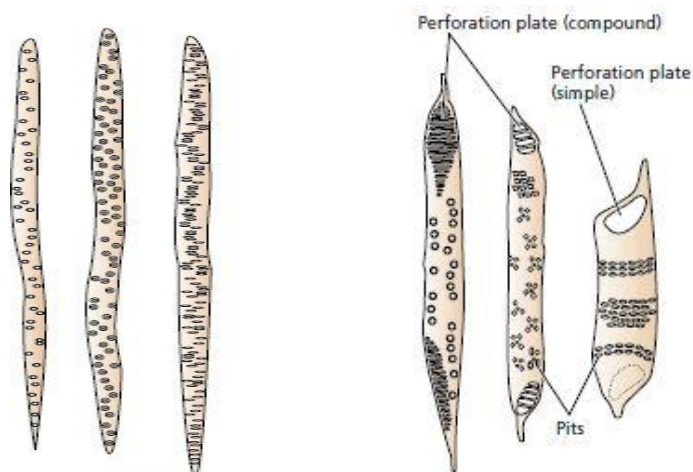


**Figure 1: Tracheids and vessel elements (simplified)** (Taiz et al., 2003).

### 1.2.1.2 Xylem structure in broad-leaved trees

The wood of broadleaf trees consists of more diverse cells with the formation of a hydro- and structural system. The mostly dead wood fibers typically form thick cell walls and show some pits. They are connected via tracheids to the hydrosystem and also show connections to the storage system, the parenchyma cells.

The main hydrosystem consists of vessel elements. There are different arrangement types of the vessels across the cross section of the xylem, which can be distinguished into ring porous, semi-ring porous, semi-diffuse porous and diffuse porous. In ring porous xylem, vessels with large diameter are formed early in the growing season and can be clearly distinguished from the smaller vessels formed later in the growing season. In diffuse porous trees, vessels can be either microporous or macroporous and are evenly distributed over the tissue formed over the whole growing season (Pallardy, 2007).

Organic products are primarily transported in sieve tubes in the living bark. These tubes have companion cells which are responsible for filling and emptying of the sieve tubes. Compared to the simple phloem transport system of gymnosperms in sieve cells and accompanying Strasburger-cells, angiosperms show a more interlinked transport system with various elements involved (Tobergte & Curtis, 2013, pp. 68-70).

### 1.2.2 Drivers of transpiration

Water loss in trees can work via two pathways. There is always diffusion of water to the outside of the plant via the cuticle. The diffusion rate depends on the concentration difference inside and outside the plant and the permeability of the cuticle. The water loss via the cuticle varies between 0.3 % (succulent plants) and 6 % (herbs and grasses) of the total transpiration and cannot be easily regulated. Most of the water leaves the plant via the stomata located on the leaves (Lösch, 2001).

The main driver of transpiration is the strong decrease of water potential along the soil plant atmosphere continuum (SPAC) at the leaf/atmosphere interface. Depending on different factors, the stomata are regulating the transpiration to a relative value of the maximum possible value determined by the water potential gradient in the SPAC. The influencing factors on stomatal aperture are:

- light,
- temperature,
- plant water potential,
- air humidity,
- CO<sub>2</sub> and
- mechanical pressure in the epidermis (Frey et al., 2010).

These factors have different influences on the stomatal aperture, but they all cause an active change in the osmotic concentration in the closing cells of the stomata. The external factors influencing the stomatal aperture always show interactions with each other and the final opening width is always a combined result of the factors mentioned above (Frey et al., 2010).

The resistance of water loss from a leaf associated with the diffusion through the stomata is called leaf stomatal resistance. The total resistance of water loss through leaves consists of the leaf stomatal resistance, the cuticular resistance and the boundary layer resistance. The boundary layer is the layer of unstirred air next to the leaf surface through which water vapour has to diffuse to reach the turbulent air of the atmosphere. It is mainly controlled by wind speed and leaf size. If wind speed is high, the moving air reduces the thickness of the boundary layer and the stomatal aperture is largely regulating the water loss. With low

wind speeds, the boundary layer thickness is high and increases in stomatal aperture show less effect on the transpiration rate (Taiz et al., 2003).

So far, a full explanation between the combined environmental factors and the effect on stomatal aperture does not exist and varies between the different plant species. Several modelling approaches exist displaying the relationship of single factors to stomatal aperture (Oren et al., 1999; Busch et al., 1998; Buckley, 2017).

### **1.2.3 Water storage capacity of trees**

Another influencing factor to the water relations of trees is the possibility that different transport pathways like roots, trunks, branches and leaves can act as water storage compartments. Capacitive discharge of water into the transpiration stream can buffer daily fluctuations in xylem tension. This effect diminishes the risk of xylem embolism and hydraulic failure under dynamic conditions during a day (Scholz et al., 2011).

The discharge of the water storage in a tree does not happen uniformly over the whole stem. Cermak et al. (2007) found that the upper parts of the stem are discharged first. In the study, the authors measured a time lag of one to two hours between sap flow starting in the upper part of Douglas fir trees compared to the base of the trees. The water balance in the morning hours after sunrise was negative and the stem storage was discharged. In the case of the study, the water balance turned positive again at 10:00 and refilled the depleted stem storage in the afternoon and at night. Simultaneous to the charge and discharge of the stem storage the diameter of the tree increased or decreased.

Köcher et al. (2013) concluded in their study of five different temperate broadleaf trees that stem storage capacity is probably most important during periods of good soil water supply. During drought, the storage is depleted rapidly and it is concluded that water storage plays an important role in stress avoidance on moist and mesic sites. On sites with xeric climate other adaptations are likely more important.

### **1.2.4 Drought stress in trees**

The main strategies plants use to deal with droughts are drought avoidance and drought tolerance. Drought avoidance means escaping the drought period via seeds or other lasting organs, so that the plant does not have to be established during times of low water availability. It can also mean that plants are establishing abilities for better water access (through a widespread root network), a better conductance within the plant for water transport and a better control on how water is released to the atmosphere. Drought tolerance is associated with the ability of plants to tolerate low water potentials within the plant and plant cells. (Frey et al., 2010).

Water deficit in the context of plants can be defined as any water content of a tissue or cell that is below the highest water content exhibited at the most hydrated state (Taiz et al., 2003). Trees possess various acclimation strategies to deal with water deficit.

The most important according to Taiz & Zeiger (2010) are the following:

- Decreased leaf area
- Stimulation of leaf abscission
- Root extension into deeper, moist soil
- Stomata close during water deficit in response to ABA.

The response of stomatal aperture to water availability is not uniform in all plants. Some plants keep their stomata open although water availability is already low (i.e. during midday) and thereby experience strong fluctuations in the water potential. This behaviour is called anisohydric regulation. Others have a higher sensibility to the plant water potential and more rapidly close their stomata preventing water loss and keeping their plant water potential relatively stable. This regulation is called isohydric and is mostly related to plants in more drought prone habitats (McDowell et al., 2008; Attia et al., 2015).

When trees cannot maintain a species-specific minimum water potential, damage and mortality can result. Allen et al. (2010) identify three mutually non-exclusive mechanisms by which drought could lead to broad-scale forest mortality:

- Death of the tree through cavitation in xylem caused by extreme heat and drought
- Reduced ability to defend against biotic agents because of protracted water stress that leads to carbon starvation.
- Warm periods create a more favourable climate for pests which occur in higher abundance and overwhelm already stressed host trees.

Modelling approaches including future temperature increases and drought periods conclude that isohydric species may show increased mortality because of their higher susceptibility to droughts and are the first trees to die in an ecosystem. However, also anisohydric species may face problems during intense droughts, as their margin to hydraulic failure is narrower and cavitation can cause destruction in water transporting tissue (N. McDowell et al., 2008). It is also likely that tall trees of old-growth forests are at the greatest risk of loss due to simulations of mortality performed by N. G. McDowell et al. (2015).

### **1.3 Simulating drought stress conditions on forest ecosystems in the Himalaya region**

Few studies have addressed the relationship between climate change and drought on forest ecosystems in the southeast Himalaya region. Poudyal, Jha, Zobel, & Thapa (2004) studied the effect of drought stress in Nepal on three tree species also present in the experiment in Bhutan. Leaf water potentials, soil moisture and leaf conductance were frequently measured over the course of three years but without the monsoon period from April until September. Another study from Ghimire et al. (2014) compared sap flow in a natural broadleaf forest and a mature planted pine forest in Nepal.

Given the threat of climate change, the importance of forest ecosystems for the wider region and the scarcity of studies, there is an urgent demand for research on the effect of drought stress on trees to better understand tree mortality patterns (Steinkamp et al., 2015; N. McDowell et al., 2008) and possible changes in plant communities in a changing climate (Bonan, 2008; Jentsch et al., 2007). As there are very few studies

on the effects of drought on forest ecosystems in the Himalayas, the effects are not well understood and there is a lack of data for climate change effects on forest ecosystems in this area (Xu et al., 2009).

Through-fall exclusion experiments are an effective method to evaluate the effect of drought stress on ecosystems.

### 1.3.1 The through-fall exclusion experiment

The main goal of the through-fall exclusion trial is to examine the drought stress resistance of different forest and tree types with the aid of a through-fall exclusion roof. There are many through-fall exclusion trials ongoing or finished all over the world to simulate drought stress and to see how the ecosystem is reacting to it. Table 1 lists through-fall experiments in only wet tropical or subtropical regions (Bonal et al., 2016).

**Table 1: A list of through-fall experiments in wet tropical or subtropical regions** (Bonal et al., 2016).

Site	Location	Climate	Period	Reference
Daintree rainforest	Australia	Seasonal wet tropical	2013–	<a href="http://www.jcu.edu.au/daintree">http://www.jcu.edu.au/daintree</a>
Caxiuanã National Forest Reserve	Brazil	Seasonal wet tropical	2002–	Fisher et al. (2007)
Tapajós National Forest	Brazil	Seasonal wet tropical	2000–	Nepstad et al. (2002)
Lore Lindu National Park	Indonesia	Aseasonal wet tropical	2007–2009	Van Straaten et al. (2011)
FazendaVitória	Brazil	Seasonal wet tropical	1993–1996	Cattânio et al. (2002)
Luquillo Experimental Forest	Puerto Rico	Aseasonal wet subtropical	2009	Wood and Silver (2012)
Golfo Dulce Forest Reserve	Costa Rica	Seasonal wet tropical	2007–2008	Cleveland et al. (2010)

Two examples of through-fall experiments in mountainous areas are trials in Middle Europe (Netherer et al., 2014; Leo et al., 2014) aiming to examine the stress reactions of the trees. So far, there has been no through-fall experiment in the Himalayan region to study drought stress reactions of the ecosystems in the area.

Results from the first years of the present trial have been already published (Wangdi et al., 2017) focussing on changing soil CO<sub>2</sub> – effluxes from both forest types examined in this experiment. Intensive characterization of the soils at both forest types has been done during the experiment including soil profiles, soil samples, soil incubation, soil respiration and climate.

### 1.3.2 Sap flow and drought stress

Sap flow measurements are used to quantify water transport in plants. There are various sensor types available that use mostly the principle of heat dissipation. Sensor types can be distinguished in systems that measure the sap flow density (cm<sup>3</sup> \* cm<sup>-2</sup> \* h<sup>-1</sup>) and those that measure sap flow rate (g \* h<sup>-1</sup>). Most of these methods share the same principle of heat dissipation by the transport of water in the plant. To measure sap flow density, two main principles are applied. The first principle of constant heating is applied for heat dissipation or thermal heat field deformation method. The second principle uses heat pulses and is applied in the compensation heat velocity, Tmax, heat ratio, calibration average gradient and Sapflow+ methods (Vandegehuchte et al., 2013).



In the experimental plots of this study only Granier-type sensors were used. These sensors use the principle of a constant heated probe and are also called Thermal dissipation probe (TDP). The aim was to equip a high number of trees on the plots with sensors to have more replications rather than applying two or more sensors on one tree to get more precise data for each individual.

Granier type sensors were used in a wide variety of experiments to measure the water household of trees. Sap flow, sap flow density or relative sap flow values are used for the characterization of water transport and transpiration by trees. Leo et al. (2014) for instance examined the drought stress reaction of three different coniferous species (*Picea abies*, *Pinus sylvestris* and *Larix decidua*) on an inner alpine site in Austria. Sap flow measurements were applied to evaluate the plant water availability and to characterize the reaction of the trees by analysing the dependency of sap flow to volumetric soil water content, irradiance and vapour pressure deficit. The authors tried to find out differences in these dependencies caused by the stress applied to the trees in the throughfall exclusion experiment. The results show clear effects of drought stress in all three studied tree species. The authors also concluded, that *Larix decidua* might be more susceptible to increased temperatures in the future because the species does not show much reduction in canopy conductance during times of high evaporative demand.

Another study in Switzerland carried out by Leuzinger & Körner (2007) used sap flow measurements to evaluate water savings under elevated CO<sub>2</sub> concentrations in a “Free Air Carbon Dioxide Enrichment Experiment” (FACE). Drought resistance of *Fagus sylvatica* was studied with the help of sap flow measurements in Denmark (Dalsgaard et al., 2011). Further studies using sap flow to examine drought induced stress in trees can be found in the literature (Gartner et al., 2009; Schäfer, 2011; Du et al., 2011).

#### **1.4 Goals and hypothesis of through-fall exclusion experiment**

In the experiment, the drought stress resistance of five different tree species was analysed via sap flow measurements. The experiment was located in two different forest types in the south-eastern Himalaya, in Bhutan. Sixty trees were equipped with Granier type thermal dissipation sensors measuring sap flow density. Other data on environmental parameters were collected by meteorological stations and soil moisture sensors.

Through-fall exclusion roofs were established to simulate monsoon failure in the forest ecosystems to study the effect of reduced water supply. One study site is located in a mixed coniferous forest where trees of *Tsuga dumosa* and *Quercus semecarpifolia*, as dominant species, and *Rhododendron arboreum*, as understorey species, were equipped with sap flow sensors. On the other study site, a broadleaf forest, *Quercus griffithi* and *Quercus lanata*, as dominant species, and again *Rhododendron arboreum*, as understorey species were measured. The interesting facts about the experiment are the differences amongst the measured tree species in terms of tree type (coniferous vs. broadleaf trees), phenology (deciduous vs. evergreen) and wood anatomy (tracheids, semi-ring-porous vessels and ring-porous vessels). There might be also differences in strategies how the different tree species react to drought and which strategies they follow.

The study on one hand tried to provide information on how the forest ecosystems react to drought stress, which might be experienced under future monsoon failures. This can be important information for policy makers who deal with climate change issues in the area to avoid severe negative effects on the forest ecosystems and communities.

On the other hand, the experiment can provide data on how tree species with very different traits react to water stress. As only limited knowledge exists on the ecology of tree species in this area, this can improve models for the simulation of the effects of climate change on forest ecosystems in a so far underrepresented region. To study the functionality of the through-fall exclusion roofs and the extent of their effect on the water relation of the trees, sap flow data of control and treatment plots are compared.

Hypothesis addressed were

(1): Trees on the roofed (stressed) plots have lower sap flow compared to trees in the uncovered control plots.

To assess the differences amongst the species more precisely, sap flow data is compared with the environmental parameters vapour pressure deficit, irradiance and soil moisture. This approach has already been used by other studies (Leo et al., 2014; Du et al., 2011; Leuzinger et al., 2007; Ghimire et al., 2014; Dalsgaard et al., 2011) because these three environmental parameter are considered to be amongst the main drivers of sap flow.

Hypothesis (2) Sap flow is strongly related to the environmental parameters vapour pressure deficit, irradiance and soil moisture.

Trees also store water in their stem and other compartments. This storage can buffer the effect of drought stress and avoid hydraulic failure (Scholz et al., 2011). Trees that show longer lags between transpiration by the leaves and changes in sap flow at the tree base appear to have a higher stem storage capacity (Čermák et al., 2007).

Hypothesis (3)

Time lags between sap flow and the environmental parameters vapour pressure deficit and irradiance differ amongst the species which is an indicator for the stem capacity of the species.

## 2 Material and methods

### 2.1 The study sites

For the study, two dominant forest-ecosystems along an altitudinal gradient in the Eastern Himalaya were selected. A cool, mixed conifer forest at an elevation of 3,200 m (in the following named after its site name Tashigang Goempa - TG) and a cool broadleaf forest at an elevation of 2,400 m (in the following named after its site name Pangsho Goempa - PG). The two study areas are located 13 km apart and consist of four plots each. Figure 2 shows the exact location of the two sites in Bhutan.

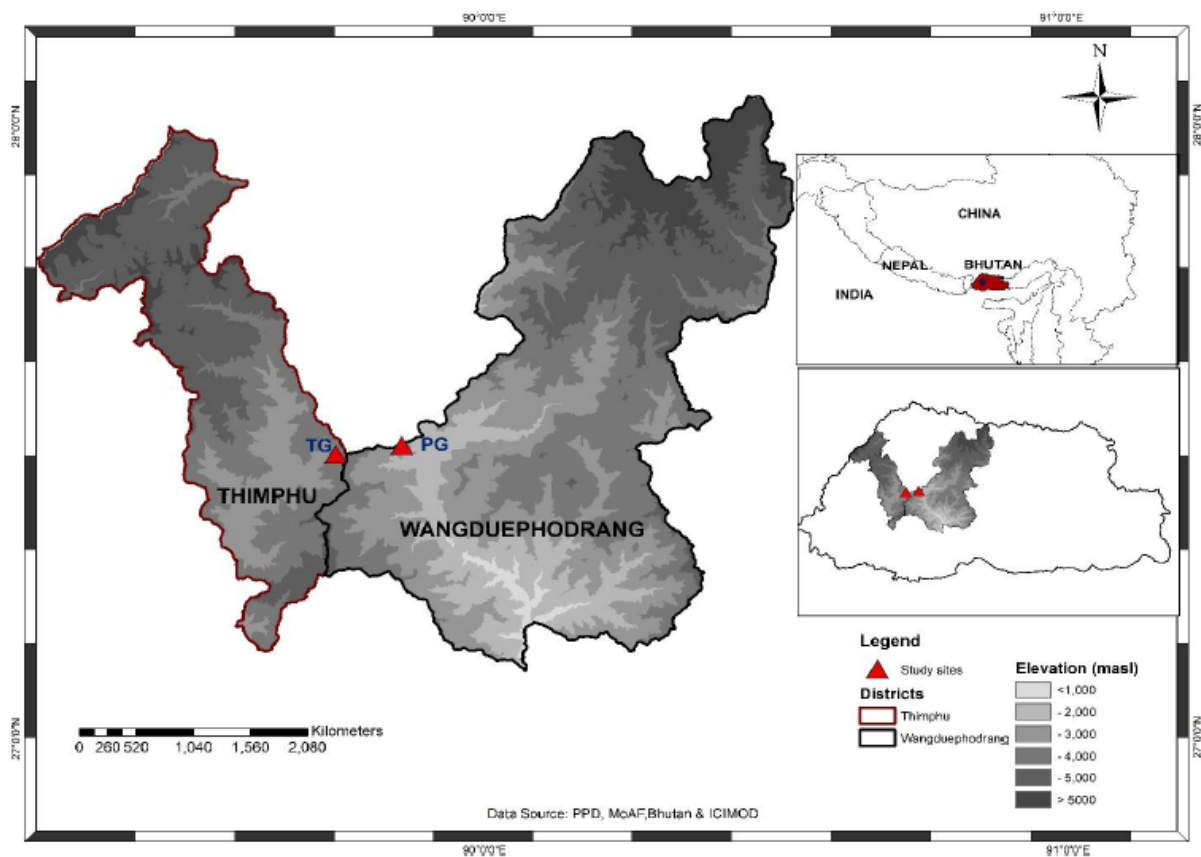


Figure 2: Location of the through-fall exclusion experiment in Bhutan (TG = Tashigang Goempa, PG = Pangsho Goempa). (Om, 2016)

**Table 2: Characteristics of experimental plots.**

Parameter	Mixed coniferous forest (TG)	Broadleaf forest (PG)
Elevation (m)	3 260	2 460
Latitude	27° 28' 00" N	28° 28' 51.06" N
Longitude	89° 44' 30.79" E	89° 81' 27.73" E
Annual precipitation (mm)	1175	1027
Mean annual temperature (°C)	8	12
Topography	concave, convex/concave	concave
Slope position	mid slope	mid slope, shoulder
Aspect	S-SSE	E-ESE
Slope	25-30°	15-25°

## 2.2 Climate and weather

Climate on both sites is characterized by dry winters and wet summers influenced by monsoon rainfalls. In Wangda & Ohsawa (2006a) five year weather data is presented along an altitudinal gradient similar to the one in the present study. The Walter climate diagrams for the two sites matching the studied coniferous forest and broadleaf forest are shown in Figure 3.

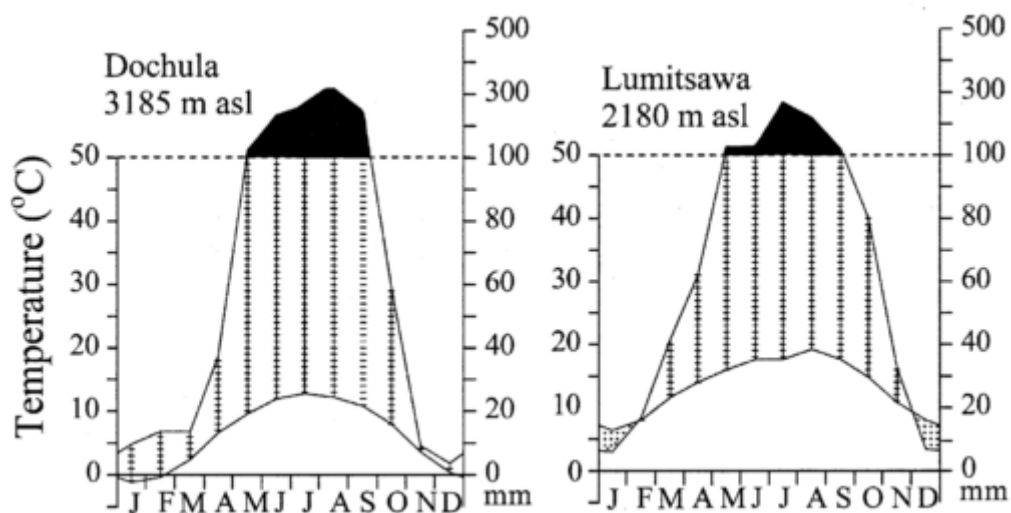


**Figure 3: Walter's climate diagram for representative sites along altitudinal gradient (Dochula - mixed coniferous forest, Lumitsawa - broadleaf forest, modified).**

(Wangda et al., 2006a)

Additionally, the weather data from the weather stations from the present study for the mixed coniferous and the broadleaf forest are shown in Figure 4. Total measured precipitation on site (from July 2014 – June

2015) was 1027 mm at the broadleaf and 1175 mm at the mixed coniferous forest. 75 % of the precipitation was recorded in the month between June and September typical for a monsoon rainfall pattern. Mean summer temperatures from June till September 2014 are 17.4 (broadleaf forest) and 13.7 °C (mixed coniferous forest). Mean winter temperatures from December 2014 to February 2015 were 6.3 °C (broadleaf forest) and 2.5 °C (mixed coniferous forest).

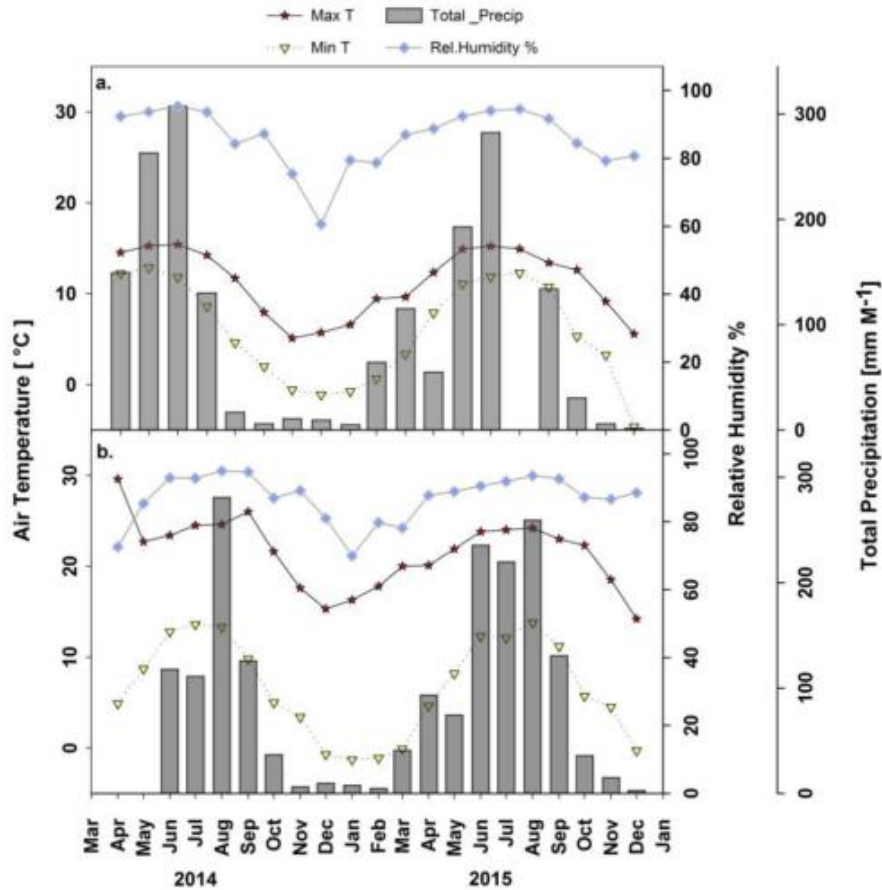


Figure 4: Monthly mean maximum air temperature [°C], Minimum air temperature [°C] and total precipitation [mm \* M<sup>-1</sup>] at the mixed coniferous forest site (a) and the broadleaf forest site (b).

(Wangdi, 2016)

Meteorological stations were established at both sites approximately one kilometre from the plots. Recorded parameters are precipitation (ECRN-100 rain gauge), net radiation (PYR solar radiation sensor), wind speed and direction (DS-2 sonic anemometer) and air temperature and relative humidity (VP-3 vapour pressure, temperature and relative humidity sensor). All meteorological instruments were purchased from Decagon Devices (USA). Signals were measured and stored by a Decagon-Em 50 data logger in a 15min interval.



Vapour pressure deficit ( $D$ ) in [kPa] was calculated from air temperature and relative humidity. For the further evaluation of the climate data daily mean values were calculated, except for precipitation, where the daily sums were used for further calculations. To exclude values measured during night, only values where the irradiance ( $E$ ) was higher than 20 W/m<sup>2</sup> were included in the calculations.

## 2.3 Soil characteristics

Table 3 shows a typical soil profile for each site and provides further information about the soil horizon characteristics.

Soils from the mixed coniferous forest site are classified as endo-skeletal Cambisols, the humus form is Moder. Soil texture is mostly loamy and the plant available water storage capacity varies from 100 mm in convex slope positions to 195 mm in concave slope positions. The soils in the broadleaf forest are characterized as endostagnic Luvisols and the humus form is Mull. The soil texture varies from silty clay in the topsoil to clay in the subsoil. Roots were only confined until a depth of 100 cm although soil depth exceeded 130 cm. The plant available water storage capacity is higher than at the mixed coniferous site with 280 mm in the whole profile or 210 mm within the rooting depth (Wangdi, 2016).

**Table 3: Soil profiles and soil horizon description for both forest types (Wangdi, 2016).**

Site	Soil Profile	Depth (cm)	Texture and Structure	Coarse soil	Colour	Rooting
 <b>Coniferous</b>	M	0-1				
	F	2.5-3.5	Layered, sticky many fungal hyphae	0		Many
	H	2-3	Loose	0		Many
	Ahbiog	0-10	Clay loam, fine to medium blocky, granular (worm casts), half open to open,	0	7.5YR3/4	Common
	ABw	10-30	Clay loam, fine to medium blocky, subangular, half open	10	7.5YR4/4	
	Bw1	30-60	Clay loam, fine to medium blocky, subpolyhedral, half open to closed,	20	7.5YR6/8	Many Few
	BwCw	60-80	Sandy clay loam, single grain to slightly coherent	50	10YR6/8	None
Cw	80-100+	Sandy clay loam	100	10YR5/6	None	
 <b>Broadleaved</b>	L/F	0-1.5	Loose			None
	Ahbiog1	0-2.5	Silty clay, loose, crumbly	0	10YR2/2	Many
	Ahbiog2	2.5-23	Loam, fine crumb to fine blocky; open	0	10YR3/6	Common
	Bw/E	23-53	Silty clay, fine to medium blocky, half open	0	10YR5/8	Common
	Bw/Bt	53-70	Clayey loam, medium blocky, closed	0	7.5YR4/3	Few
	Bth	70-100	Clay, blocky polyhedral, closed	0	10YR2/2	Very few
	Btgc	100-130+	Clay, coarse blocky-polyhedral, closed	0		None

Every third week soil volumetric water content ( $SWC_v$ ) and temperature measurements were taken on a 5 x 5 m grid for the whole plot area using a handheld TDR (Field Scout 100, Spectrum Technologies, USA) for  $SWC_v$  measurements and a handheld thermometer probe (Hana Instruments, Germany) for soil

temperatures. Furthermore, at the center of each plot, SWCv and soil temperature probes (five 5TM soil moisture sensors) were mounted in fixed depth (between 5 and 120 cm – depending on soil depth) for each plot to have continuous records over time. A Decagon 50 datalogger was used to store the signals. Additionally, at the coniferous forest site, a GS3 sensor (Decagon Devices, USA) was mounted to store SWCv data in the humus layer at 2 cm depth. The interval for all continuous measurements was 15 min.

Because of the heterogeneity of the soil depth at the Tashigang Goempa site there is a variation in the mounting depth of the SWCv and soil temperature sensors. The sensors were distributed to a minimum depth of 50 cm according to the circumstances at the plot. As soil depth at the Pangsho Goempa site is in general deeper for all plots, the sensors were placed at the same depth at every plot. The distribution of the sensors is given in Table 4.

**Table 4: Distribution of SWCv sensors in the soil profiles at all plots.**

Sensor depth in profile [cm]	Sensor types at Tashigang Goempa site				Sensor types at Pangsho Goempa site			
	TG1C	TG2T	TG3C	TG4T	PG1C	PG2T	PG3C	PG4T
0	GS3		GS3	GS3				
5	5TM	5TM	5TM	5TM	5TM	5TM	5TM	5TM
20	5TM	5TM	5TM	5TM	5TM	5TM	5TM	5TM
40			5TM					
50	5TM	5TM	5TM	5TM	5TM	5TM	5TM	5TM
70		5TM						
90	5TM	5TM		5TM	5TM	5TM	5TM	5TM
120					5TM	5TM	5TM	5TM

(TG = Tashigang Goempa, PG = Pangsho Goempa, C= Control, T= Treatment (roof) plot)

## 2.4 Examined tree species

The dominant species in the mixed coniferous forest are *Tsuga dumosa* and *Quercus semecarpifolia* (evergreen) in the overstorey and *Rhododendron arboreum* in the understorey. The broadleaf forest site is dominated by *Quercus griffithi* (deciduous) and *Quercus lanata* (evergreen) and again *Rhododendron arboreum* in the understorey. As mentioned above, the forest types are aligned on an altitudinal gradient of a typical dry valley of the Eastern Himalayas. The forest types along this altitudinal gradient are well documented by Wangda & Ohsawa (2006) giving the distribution of dominant tree species.

Between 3000 to 3200 m the limit for *Tsuga dumosa* and *Quercus semecarpifolia* is reached. This altitude also marks the end of the cool-temperate zone and the beginning of the cold-temperate zone. This elevation was selected for study area one, the coniferous forest. At lower altitudes *Quercus semecarpifolia*, *Quercus glauca* and *Quercus oxyodon* become the dominant tree species. At an altitude of 2 540 m *Quercus griffithi* and *Quercus lanata* are dominant. This is the elevation of the second study area, the broadleaf forest. Below 1 860 m, *Pinus roxburghii* is becoming the dominant tree species (Wangda et al., 2006b).

*Rhododendron* species are the most abundant trees in absolute numbers in Bhutan (nearly 90 million individuals) followed by *Quercus* species (86 million individuals). *Tsuga dumosa* is the twelfth most abundant with around 12 million trees in Bhutan (MoAF, 2017).



Figure 5: Mixed coniferous forest site in Bhutan/Thimphu district.

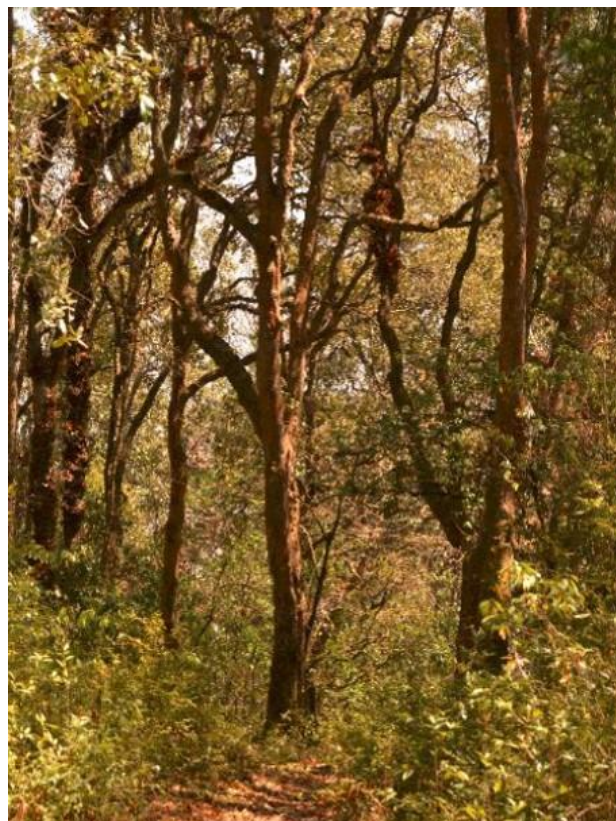


Figure 6: Broadleaf forest site, Bhutan/Wangdue Phodrang district.



## 2.5 The through-fall exclusion experiment

As part of the BCCAP-project (Bhutan Climate Change Adaptation Program) the through-fall exclusion experiment was set up to study the effect of partial or full monsoon failure on forest ecosystems. Several experiments were done on the research plots to study the effects of simulated drought on the selected ecosystems starting in 2014. The sap flow measurement system was part of the initial setup but for this study only the period from September 2016 till December 2016 was chosen as the download frequency and data quality was highest during this time.

### 2.5.1 The through-fall exclusion roofs

On each plot two 25 m x 29 m roofs at an average height of 2.5 m were mounted. A wooden construction was covered with plastic foil and 1.5 m trenches were dug upslope of the roofs. The plastic foil is UV-stabilized, cross laminated polyethylene and has 80-86 % transparency for photosynthetic active radiation. The first period with established roofs started on the first of May 2014 and lasted till 28<sup>th</sup> of August 2014 to simulate a partial monsoon failure. In 2015 the period with established roof lasted from April till October to simulate a full monsoon failure. In 2016 the roofs were again mounted in May and remained until the beginning of December 2016 to put further stress on the ecosystems.



Figure 7: Wooden structure without plastic foil at the broadleaf forest site, Bhutan/Wangdue Phodrang district.

According to the results of Wangdi (2016) the first year of measurements in 2014 with the roofs mounted from 1<sup>st</sup> of May till 28<sup>th</sup> of August showed a reduction of through-fall at the mixed coniferous site of 75 % (863 mm) and 68 % (608 mm) at the broadleaf site.



**Figure 8: Roof with plastic foil at the broadleaf forest site, Bhutan/Wangdue Phodrang district.**



**Figure 9: Roof at the mixed coniferous site, Bhutan/Thimphu district.**



Figure 10: Trenches at roof plots to avoid water flow from upslope.

### 2.5.2 Sap flow measurements

In total 60 sap flow sensors were installed on both sites of the experiment. Five individuals of *Quercus semecarpifolia*, nine individuals of *Quercus griffithi*, twelve individuals of *Quercus lanata*, 17 individuals of *Rhododendron arboreum* and 17 individuals of *Tsuga dumosa* were selected for sap flow measurements (see Table 6). For the study, the period from August 2016 till November 2016 was chosen. From August till the beginning of October weather was influenced by regular monsoon rainfall and a change of sunny and cloudy conditions. After mid-October, rainfall mostly stopped and the weather was dominated by clear sky conditions. To apply further stress on the trees, the roof was left longer in place in 2016 and was dismantled on both sites by the beginning of December 2016.

Table 5: Number of individuals per species and site included in the study.

Tree species	n roof	n control	n total
Mixed coniferous forest (Tashigang Goempa)			
<i>Tsuga dumosa</i>	9	8	17
<i>Quercus semecarpifolia</i>	3	2	5
<i>Rhododendron arboreum</i>	4	4	8
Broadleaf forest (Pangsho Goempa)			
<i>Quercus lanata</i>	6	4	10
<i>Quercus griffithi</i>	4	6	10
<i>Rhododendron arboreum</i>	4	4	8

Table 6: List of trees with sap flow sensors (Wangdi, 2016).

Tashigang Goempa					Pangsho Goempa				
Plot	Tree				Plot	Tree			
	No.	Species	dbh(cm)	Height(m)		No.	Species	dbh(cm)	Height(m)
TG1C	49	<i>Q. semecarpifolia</i>	75	36	137	<i>Q. griffithii</i>	37	27.6	
	44	<i>Q. semecarpifolia</i>	89	26	141	<i>Q. griffithii</i>	29.2	26.3	
	42	<i>R. arboreum</i>	14.5	6	185	<i>Q. griffithii</i>	42.5	24.9	
	40	<i>R. arboreum</i>	11	6	188	<i>Q. lanata</i>	40	25	
	39	<i>R. arboreum</i>	10	5	PG1C 189	<i>Q. lanata</i>	42.5	25.3	
	38	<i>T. dumosa</i>	50	24	187	<i>R. arboreum</i>	27	11.9	
	37	<i>T. dumosa</i>	44	26	149	<i>R. arboreum</i>	21	10.2	
	50	<i>T. dumosa</i>	32	30	199	<i>R. arboreum</i>	17.5	12.4	
	48	<i>T. dumosa</i>	58	37					
TG2T	57	<i>Q. semecarpifolia</i>	86	31	219	<i>Q. griffithii</i>	29.5	21.1	
	70	<i>R. arboreum</i>	12.5	8	118	<i>Q. griffithii</i>	55	35.5	
	68	<i>R. arboreum</i>	12.5	8	221	<i>Q. lanata</i>	67.5	22	
	65	<i>R. arboreum</i>	21	9	128	<i>Q. lanata</i>	68.7	16.6	
	56	<i>T. dumosa</i>	51	27	PG2T 211	<i>R. arboreum</i>	23	9.7	
	67	<i>T. dumosa</i>	35	23	129	<i>R. arboreum</i>	16.5	6.6	
	63	<i>T. dumosa</i>	33	21	207	<i>Q. lanata</i>	57.8	27.9	
	74	<i>T. dumosa</i>	31.3	23					
	TG3C	178	<i>Q. semecarpifolia</i>	86	34	256	<i>Q. griffithii</i>	56.5	23.9
181		<i>R. arboreum</i>	13	6	242	<i>Q. griffithii</i>	37	20.4	
160		<i>R. arboreum</i>	13	6	234	<i>Q. griffithii</i>	41	39.4	
177		<i>T. dumosa</i>	52	37	PG3C 255	<i>Q. lanata</i>	50	18.6	
174		<i>T. dumosa</i>	96	41	249	<i>Q. lanata</i>	38	19	
179		<i>T. dumosa</i>	46	33	233	<i>Q. lanata</i>	79	32.3	
171		<i>T. dumosa</i>	97	37	235	<i>R. arboreum</i>	22	9.7	
TG4T	103	<i>Q. semecarpifolia</i>	36.5	22	272	<i>Q. griffithii</i>	45	15.5	
	90	<i>R. arboreum</i>	18.5	10	277	<i>Q. griffithii</i>	52	24.4	
	91	<i>T. dumosa</i>	90	35	295	<i>Q. griffithii</i>	67	19	
	93	<i>T. dumosa</i>	75	32	PG4T 281	<i>Q. lanata</i>	65.5	27	
	100	<i>T. dumosa</i>	37	23	314	<i>Q. lanata</i>	75	21.5	
	101	<i>T. dumosa</i>	59	29	274	<i>R. arboreum</i>	11	10.2	
	102	<i>T. dumosa</i>	25	17	279	<i>R. arboreum</i>	11.5	8.5	
					282	<i>R. arboreum</i>	12.8	11.4	

TG: Tashigang Goempa, PG: Pangsho Goempa, C: Control, T: Treatment (roof) plot, dbh: diameter at breastheight

### 2.5.2.1 Measurement setup

Sap flow was measured using Granier-type thermal dissipation sensors. This method for measuring sap flow in a stem was first developed by Granier (Granier, 1985). The Granier system consists out of two sensor probes and a datalogger to measure voltage differences. The probes are mounted radially on the stem with a distance between 10 -15 cm to each other.

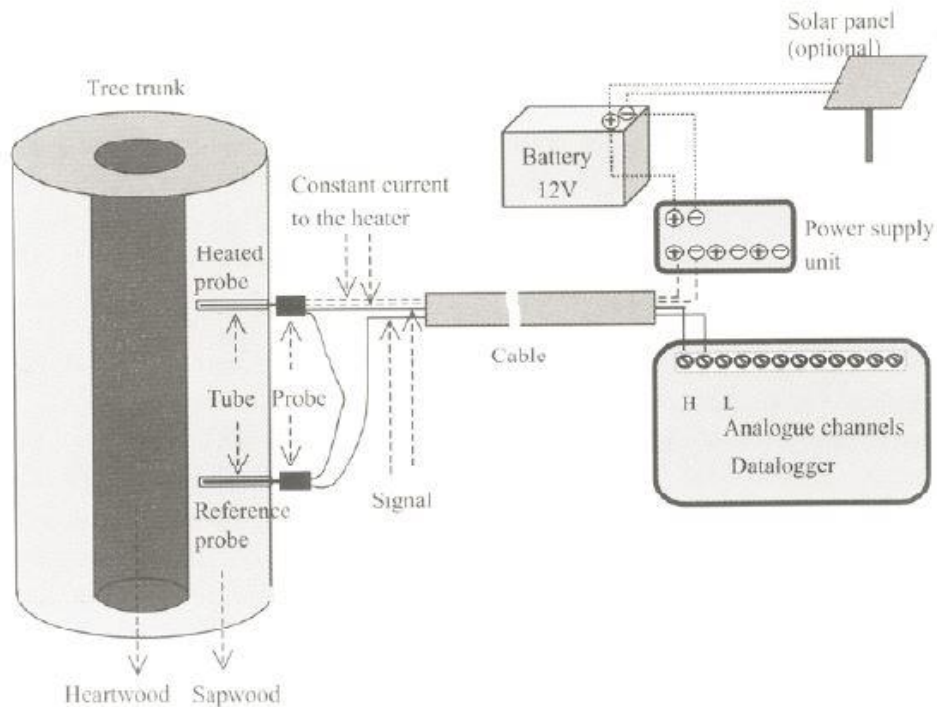


**Figure 11: Schematic overview of Granier system for sap flow measurements.** (Lu et al., 2004)

When the method was developed a comprehensive calibration was done on three different tree species leading to the correlation between measured temperature difference between the two probes and sap velocity (Clearwater et al., 1999). Figure 12 shows this non-linear relationship between temperature difference and sap flow.

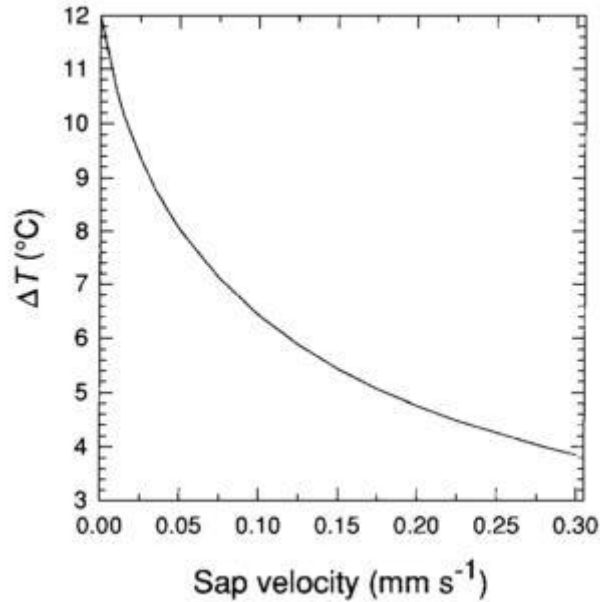


Figure 12: Temperature difference between heated and unheated probe as a function of sap flow velocity. (Clearwater et al., 1999) based on (Granier, 1985)

The schematic overview of the measurement system applied in the experiment in Figure 13 provides a simplified image about the setup in the field. Each plot has its own power socket which is connected to the grid. The data logger, charge controller, battery guard and regulators are stored in a sealed electrical box to be protected from environmental influences. Each regulator supplies one to three sensors and provides the desired current flow for the heating wires of the sensors. The sensor wires are connected to the data logger which records the signal of the thermocouples.

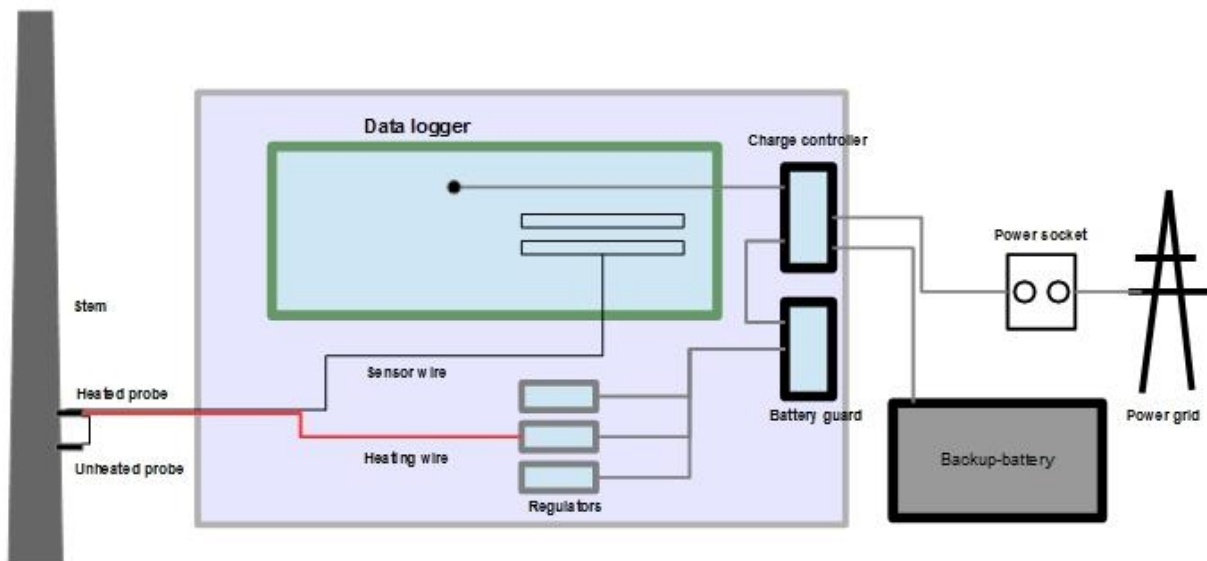


Figure 13: Schematic overview of the measurement setup at every plot.

### 2.5.2.2 Power supply

After facing several problems with the power supply for the data loggers and sensors during the first two years of the project, a further adaption of the setup was undertaken. Each plot is equipped with a power socket which is directly connected to an established power line to the close-by monasteries. A charge controller (CH 150, Campbell Scientific, Shephed UK) is directly connected to the power line. It permanently charges a backup battery (lead-acid batteries - 60 to 80 Ah capacity) which will provide sufficient power for at least 9 days if there is a problem with the fixed power line.

The data logger is supplied directly via a 12 Volt output of the charge controller. The regulators for the heating are connected to another 12 Volt output channel of the charge controller with a battery guard mounted in-between. The battery guard will automatically disconnect the regulators and therefore the heating of the sensor if the voltage from the backup-battery drops below 12 Volt to protect the batteries from very low discharge.

### 2.5.2.3 Sap flow sensor design

The sensors used in the experiment are Granier-type Thermal Dissipation Probes (TDP) produced at the Botany Institute at BOKU University. The probe which is mounted at the higher position on the stem is additionally equipped with a heating wire. The wire has a resistance of 40 Ohms and is supplied with a constant current flow of 85 mA. The current is set at the regulator with a variable potentiometer. After connecting one to three sensors (always connected in series) to the regulator the potentiometer is adjusted to the required 85 mA. As long voltage remains stable and the resistance of the heating wires does not change, the 85 mA provide constant heating of the upper probe.



**Figure 14: Close-up of applied Granier-type sap flow sensor and drillers for perforating tree stems.**

Figure 14 shows the measures of the applied Granier-type sap flow sensors. The heating wire in the sensor starts 0.5 cm from the tip and heats the sensor on a length of 2 cm. The area between 2.5 cm and 3.5 cm remains unheated. To place the sensors in the right position, the holes drilled into the active xylem had a depth of 2.5 cm.

#### 2.5.2.4 Data logger

The data was recorded with CR1000 data loggers (Campbell Scientific, Shepshed UK:). Measurement values were taken every five seconds and then averaged over a period of 15 minutes. Data was downloaded every three weeks during the regular field visits. In the period of adjustment of the power supply and replacement of the sensors between July and September 2016, data was downloaded more frequently. The temperature difference between the two thermocouples was measured as the differential voltage signal between the upper and the lower thermocouple. Additionally to the sensor signals, also temperature of the data logger and the voltage input signal from the charge controller/battery was recorded. This input signal equals the voltage signal supplying the regulators for the heating wires.

#### 2.5.2.5 Mounting of sensors in the field

The placement of the sensors is a crucial point for the quality of the sap flow measurements. Though the Granier-type sensors are not very susceptible in terms of spatial arrangement (only 10-15 cm distance in axial has to be considered), there have to be several things taken into account when placing a sensors on a tree (Vandegehuchte et al., 2013).

a) depth of sapwood:

The inserted needle has to be fully surrounded by active sapwood, otherwise an underestimation of the sap flow is very probable. To deal with such a problem, the measured values can be corrected with **Fehler! Verweisquelle konnte nicht gefunden werden.** if the depth of active sapwood is known (Clearwater et al., 1999).

**Equation 1:** 
$$\Delta T_{sw} = \frac{\Delta T - b\Delta T_m}{a}$$

$\Delta T_{sw}$  = Temperature difference in the sap wood [K]

b = proportion of needle inserted in inactive xylem [-]

a = proportion of sensor inserted in active xylem [-]

$\Delta T$  = Temperature difference of thermocouples

$\Delta T_m$  = Temperature difference of thermocouples zero sap flow velocity [K]

b) strong radial gradient of sap flow

If there is moderate radial variation in  $v$  (sap flow density) across the depth of the sapwood as for instance in many coniferous and diffuse-porous trees, and the probe does not touch any inactive xylem, deviations will be very small. Experiments showed that if there was a twofold difference of  $v$  in the measured sapwood the error is not higher than 6 % (Lu, 2001). However, some ring-porous trees show a very uneven radial pattern of  $v$  which can be assumed to be a similar situation as the sensor would have contact to inactive



xylem (Lu et al., 2004). Such a situation could cause comparable misinterpretations of the sap flow as mentioned in point a) and therefore would require a correction of the data. Figure 15 illustrates some examples of spatial differences in sapwood in different tree species. Nadezhdina, Cermák, & Ceulemans (2002) also witnessed variations in sap wood activity and emphasis that right placement of the sensor is a crucial element for getting reliable data.

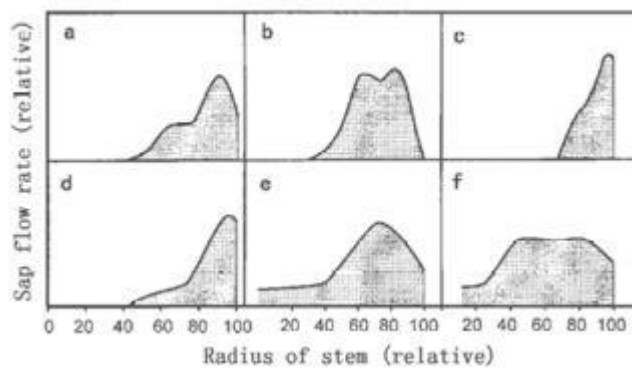


**Figure 15: Radial patterns of relative active sapwood in different tree species, 100 represents the layer immediately beneath the cambium (a = *Pinus sylvestris*, b = *Populus hybrid*, c = *Quercus petraea*, d = *Olea europea*, e = *Ficus carica*, f = *Shorea sumatrana*).**

(Lu et al., 2004)

### c) Wounding effect

"Wounding effects" can cause further misinterpretations of the sap flow. Loose connections of the probes (especially the heated probe), destruction of the xylem around the probe while placing the sensor, an unstable power supply for the heating system and insufficient insulation of the probes against wind and rainwater can cause problems with the signal and therefore deliver unsatisfactory results. This draws high attention to the right position of the sensor in the tree stem and accurate and precise working during the placement procedure (Clearwater et al., 1999; Lu et al., 2004).

In this study, one sensor was placed on each tree selected for sap flow measurements. As full calculation of transpiration was not the main goal of the experiment, single-point-measurements are considered sufficient to represent the transpiration activity of a tree. This approach has also been applied in other studies to analyse differences in transpiration (Dalsgaard et al., 2011; Leuzinger et al., 2007). However, placement of the sensor has to be done with high precision so as not to touch the inactive xylem or unnecessarily damage sap wood (Nadezhdina et al., 2002; Lu et al., 2004).

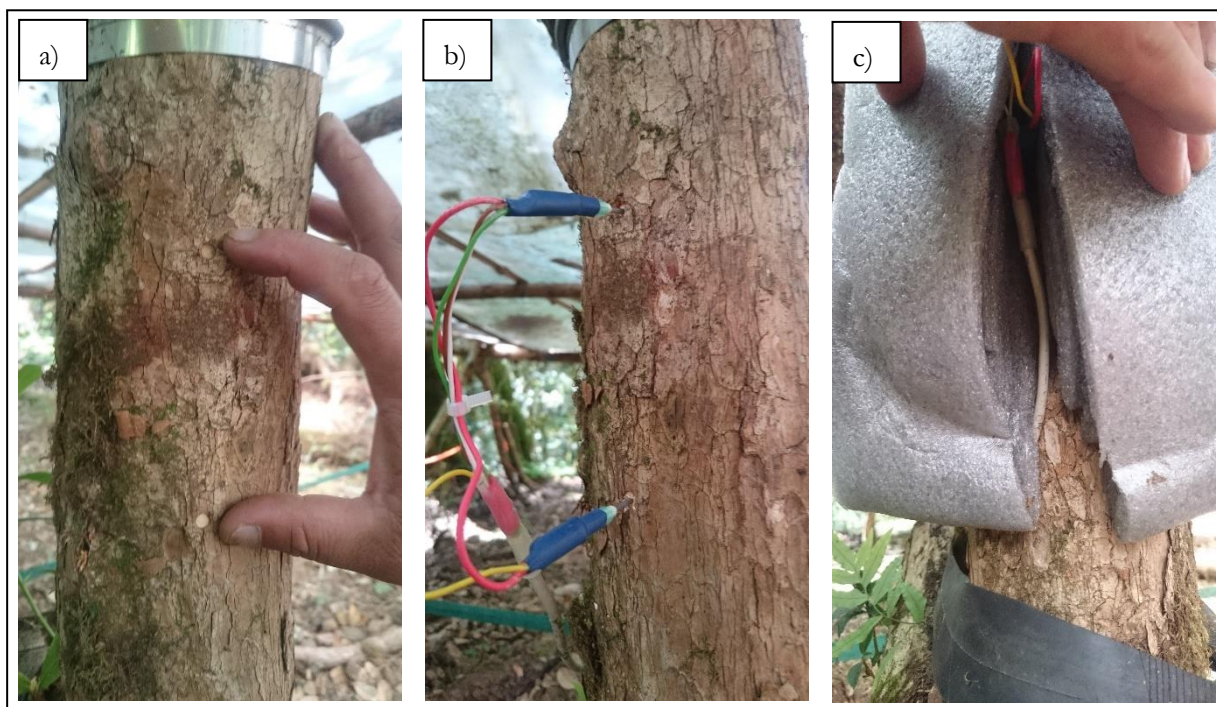


**Figure 16: Mounting procedure of sap flow sensors during field work. a) tree stem with removed bark; b) mounted sap flow sensors without cover; c) mounted sensors with insulation.**

For thermal insulation of the sensors to fluctuations in ambient temperature an insulating plastic mat was wrapped around the sensors. Additionally, to prevent thermal fluctuations from irradiance and mechanical damage, a solid plastic cover with aluminium coating was applied.

## 2.6 Data analysis and corrections

Data was analysed with R (R Development Core Team, 2016) and RStudio (RStudio Team, 2016) was utilised. For additional calculations and visualisation Microsoft Excel (2016) and plotly (<https://plot.ly>) were used. For calculations in R, the packages xts (J. A. Ryan et al., 2014), zoo (Zeileis et al., 2012), corrplot (Wei et al., 2016) and plantecophys (Duursma, 2015) were additionally applied to the standard R package.

### 2.6.1 Correction of sap flow signals

The output signal of the sensors can be disturbed by various factors. In some cases, where the cause of the bad signal was not known, or a correction was not possible, the values were not included in the evaluation. This was the case for:

- broken sensors,
- water from heavy rainfall affecting the temperature gradient between the thermocouples,
- very fluctuating signals due to dry sap wood in water stressed trees.

Due to fluctuations in the input voltage signal of different cause (black-out, hardware failure, etc.) heating energy for the sensors was not always constant. If possible, the voltage signals were corrected, using the

measured input voltage to the system. However, this was only possible for blackouts that did not last longer than a couple of days (depending on the state of the backup battery) and where the Voltage only dropped a few Volts.

To correct these wrong values, all signals were divided by the input voltage value and multiplied with a constant voltage value. The constant voltage value was chosen as an average of the measured input voltage. The results of this first correction are shown in Figure 17.

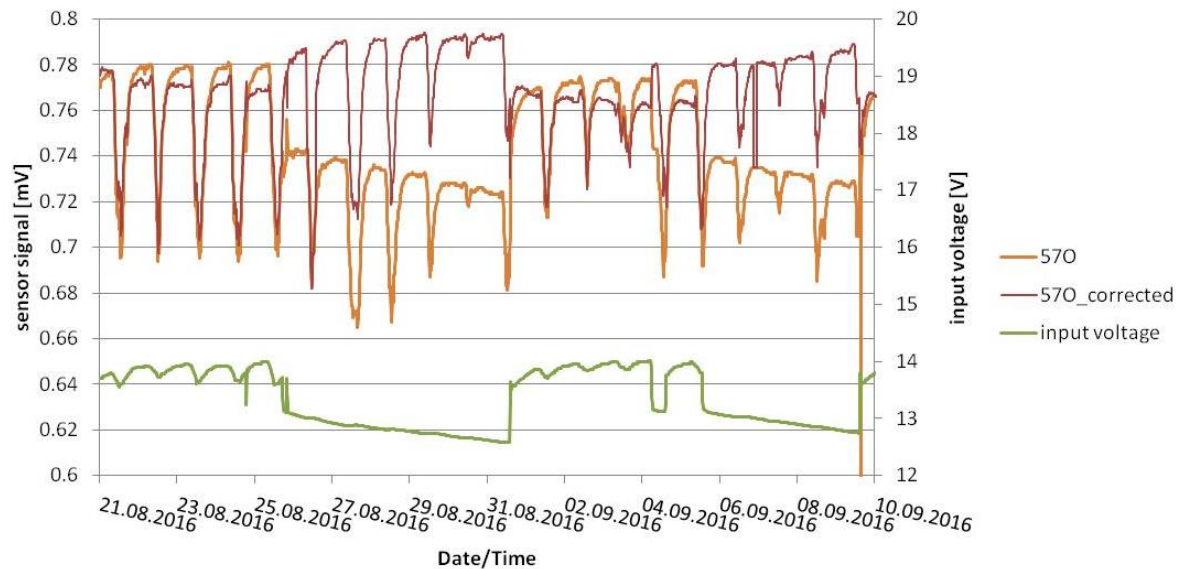


**Figure 17: Simple correction of sensor signal according to input voltage.**

The bottom line (green) in the diagram shows the results for the input voltage from the charge controller. It shows a cyclic behaviour which is due to temperature differences at the plots. If temperature is low, the charge controller increases the voltage for the system to have an ideal charging status of the battery. Unfortunately, this also influences the heating energy of the sensors and therefore has to be corrected.

Between the 26<sup>th</sup> of August and the 1<sup>st</sup> of September 2016 as well as between 5<sup>th</sup> of September and the 10<sup>th</sup> of September a hardware malfunction in the power supply system occurred and the backup battery was powering the system. During this period, the input voltage dropped from values between 13.5 and 14 Volts (provided from the charge controller) to 12.9-12.5 Volts (provided from the backup battery). This voltage drop causes less heating energy which can be observed in a drop of sensor signal during these periods (orange line). A simple correction of this effect as described above results in the red line in the diagram. The voltage drop is buffered, but there are still deviations visible from the original baseline of the signal. The signal is clearly over-pronounced. To acquire better correction factors, the time period during the first black out in Figure 17 was further analysed.

For this purpose, the ratio of the sensor signal [mV] to the input voltage [V] was taken. Figure 18 shows the mV/V-signals for the sensor from tree 57O (*Quercus semecarpifolia*) for each day in this period at 04:00 in the

morning. It is assumed that during this time no sap flow is occurring and the values should be very similar for this period.

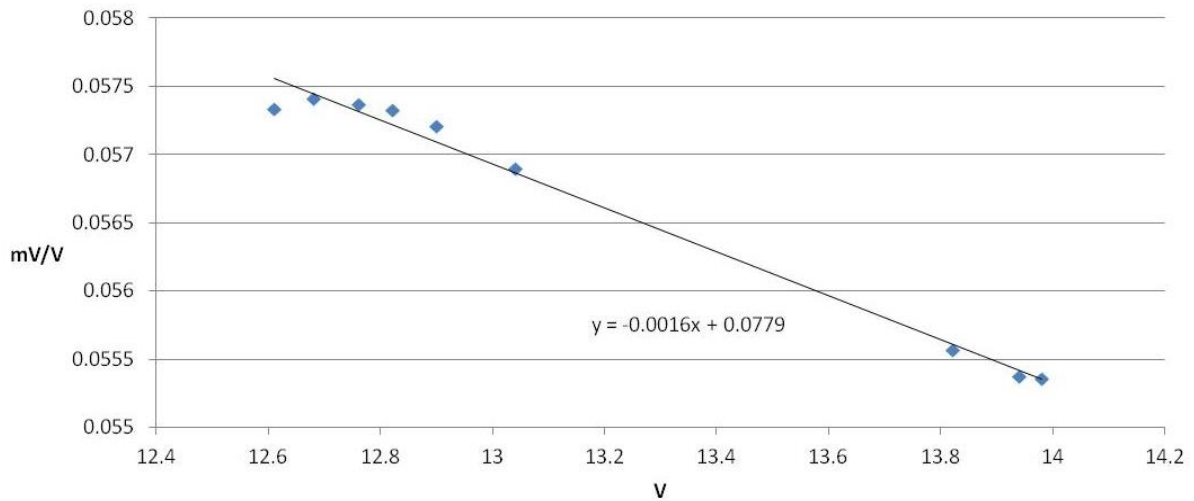


**Figure 18: Comparison of 04:00 AM values for sensor 57O during blackout.**

The distribution of the measurement points in Figure 18 indicates that there is a trend in the measured mV-signals according to the input voltage. It is assumed, that this trend comes from the difference in the heat balance if varying heating energy (due to the voltage fluctuations) is provided.

Using the values from the generated formula from Figure 18 to implement a second correction factor, the corrected values fit better to fill the gaps with fluctuating voltage.

**Equation 2:** 
$$signal_{corrected} = \frac{signal_{raw}}{input_V} * 13.8 * \left( \frac{(13.8 * e + f)}{input_V * e + f} \right)$$

inputV = Input Voltage in [V]

e = = derived from formula in Figure 18 (-0.0016)

f = = derived from formula in Figure 18 (0.0753)

The results for this second correction are shown in Figure 19. The corrected measurement values are more continuous and are used for further calculations.

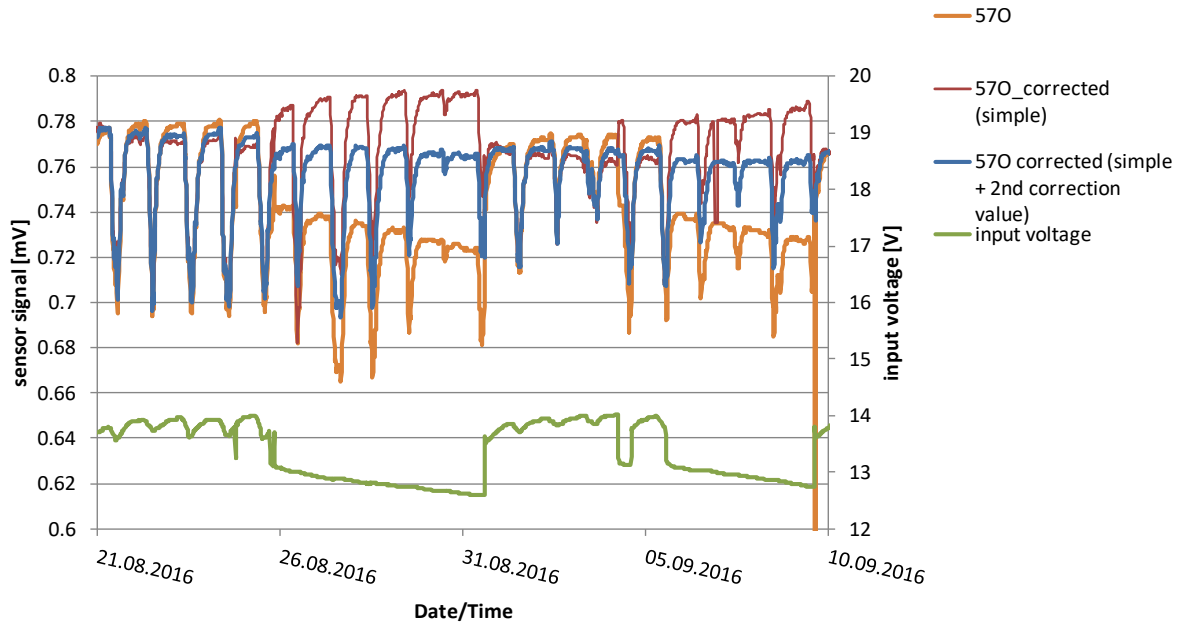


Figure 19: Corrected mV-signals for sensor 570 after implementation of second correction factor.

### 2.6.2 Calculation of sap flow density ( $Q_s$ )

After the raw Voltage signal was corrected,  $Q_s$  was calculated as (Granier, 1985)

$$\text{Equation 3: } Q_s = 0.714 * \left( \frac{dT_0 - dT}{dT} \right)^{1.231}$$

$Q_s$  = Sap flow density [ $\text{cm}^3/\text{cm}^2 * \text{min}$ ]

T = Kelvin [K]

$dT_0$  = Temperature difference between thermocouples at zero sap flow

$dT$  = Temperature difference between thermocouples

To calculate the correct values for  $Q_s$  first the temperature differences for each day at zero sap flow ( $dT_0$ ) have to be determined. Zero sap flow is taken at night as the highest mV-value (representing the highest temperature difference between the two sensors) for each day. Using the measured temperature differences ( $dT$ ) and the empirical values from the Granier experiment allows to calculate  $Q_s$ . Absolute sap flow rates were not calculated from  $Q_s$  because there was no data available concerning activity and depth of sap wood. Still, for the comparison of different tree species and the effect of the through-fall exclusion it is not necessary to calculate absolute sap flow (Leo et al., 2014).

The results of  $Q_s$  for one week in October in comparison to  $D$  and  $E$  are given in Figure 20 and Figure 21. This week marks the end of the monsoon season for 2016. At the beginning of the week on the 14<sup>th</sup> of

October 2016, there was still some rain, and  $E$  as well as  $D$  are lower. The following days, the weather was more stable with higher temperatures and  $E$ .

The calculated  $Q_s$  in Figure 20 and Figure 21 represents the mean value for all individuals per species. In this week, the signal from the roof-plots is lower than the signal from the control plots representing a lower  $Q_s$  for the trees under the roof.

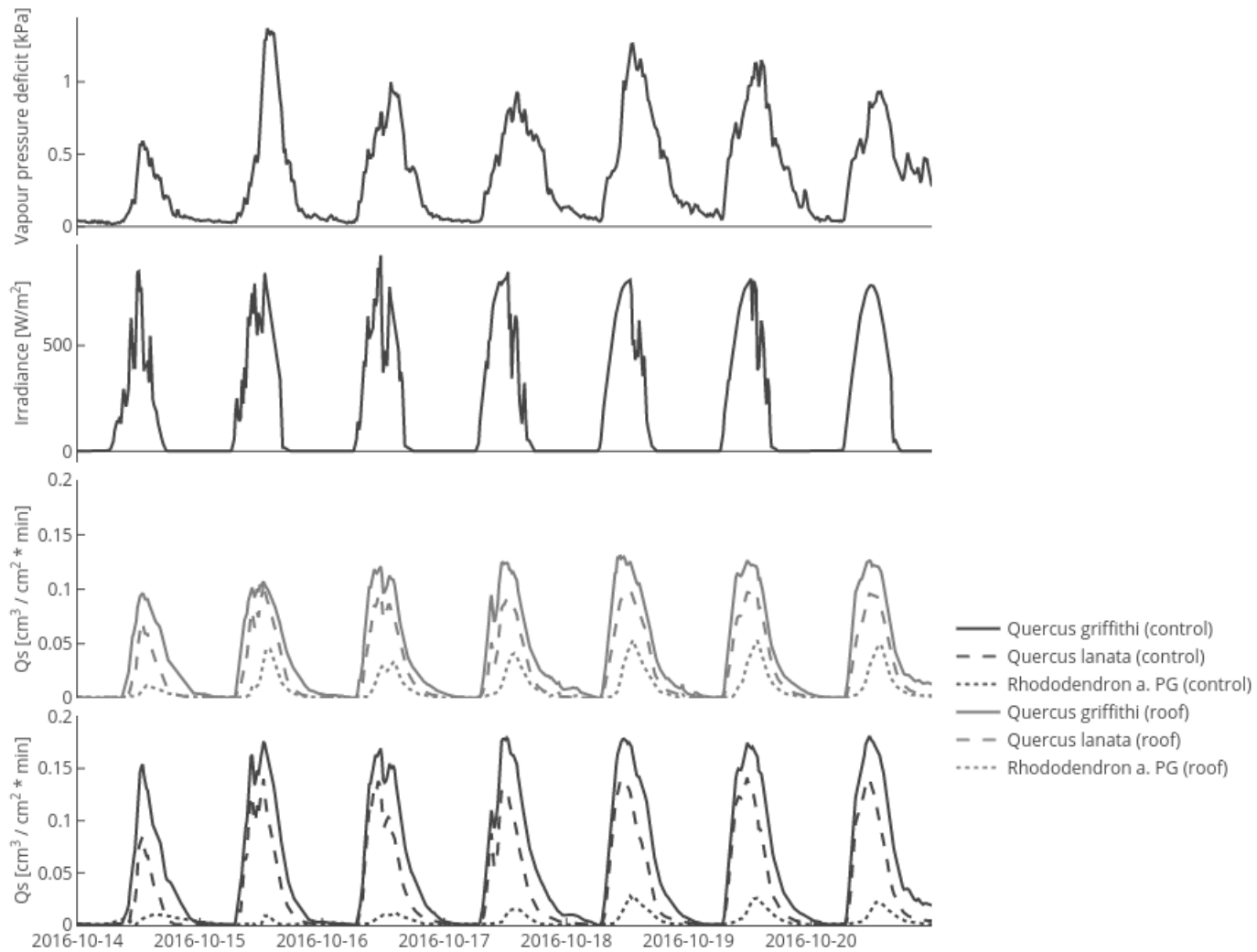
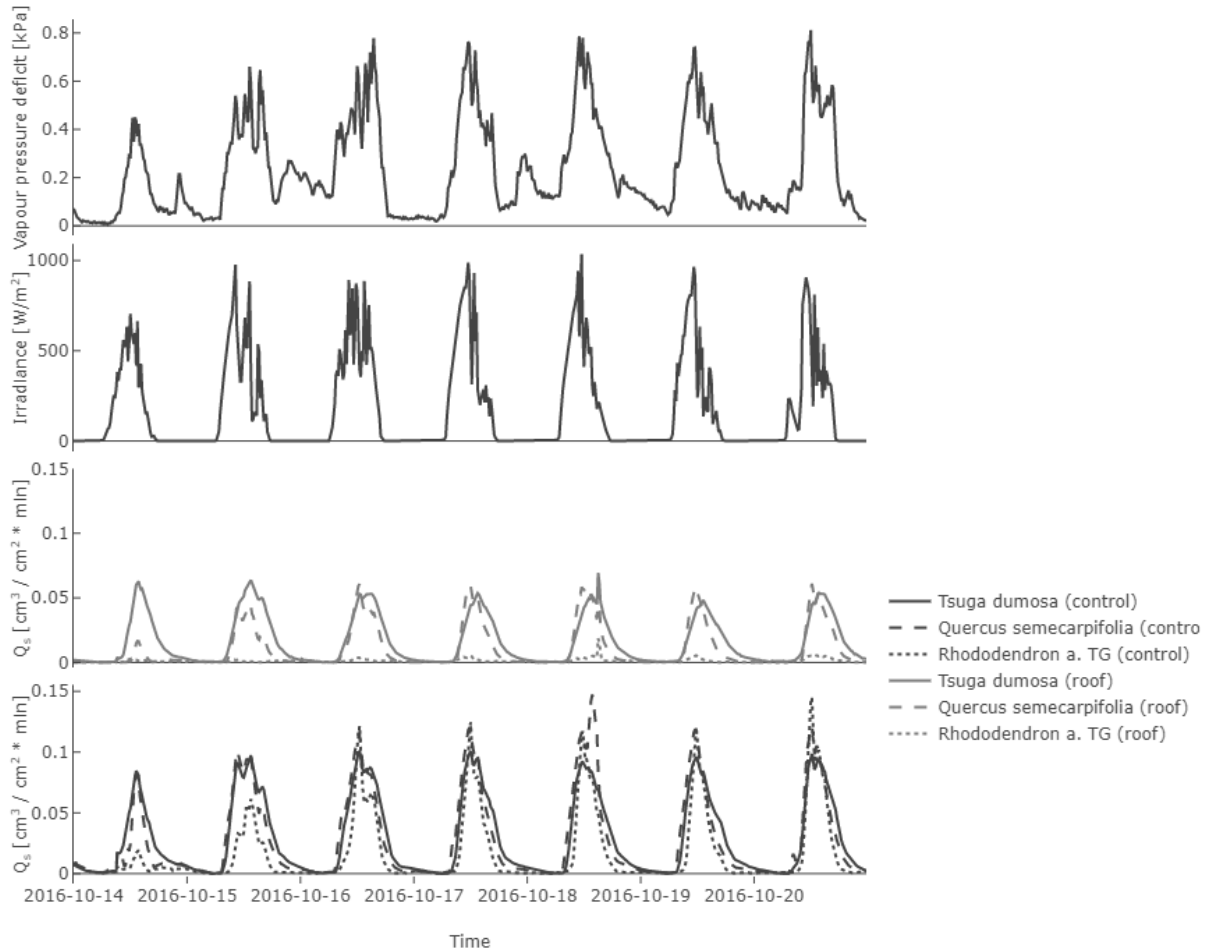


Figure 20: Calculated  $Q_s$  of trees at the broadleaf forest site (Pangsho Goempa = PG) separated by treatment and in comparison to  $D$  and  $E$ .



**Figure 21: Calculated sap flow density of trees at the mixed conifer forest site (Tashigang Goempa = TG) separated by treatment and in comparison to *D* and *E*.**

### 2.6.3 Calculation of normalised $Q_s$ ( $Q_{s-sum}$ )

For most of the statistical analysis and visualization of the sap flow density data, the normalised daily sums of  $Q_s$  per tree species were applied. First all  $Q_s$  values were filtered to only include values during day time where  $E$  was higher than  $20 \text{ W/m}^2$ . From these values, the sum for each day for each tree was calculated ( $Q_{s-sum}$ ).

To calculate normalized  $Q_{s-sum}$  ( $Q_{s-nor}$ ) the mean of these values over the whole measurement period was taken and used as a base for the calculation of the normalised values. By this step, the intra-specific variations are eliminated and a better comparison between the species is possible. This approach has already been used in several studies dealing with sap flow (Luis et al., 2005; Du et al., 2011; Leo et al., 2014). By using the mean value of the whole measurement period as a base for the calculation of standardized values, the differences between control and treatment plots were eliminated. Finally, mean values for all normalised daily sums separated by tree species and treatment were calculated.

For future evaluations of longer periods of sap flow in the present experiment a period before the mounting of the roof can be used as a base for the calculation of  $Q_{s-nor}$ , but for this study only three months of data when the roof was already established were available.

#### **2.6.4 Calculation of sap flow time lag**

To evaluate the water capacity of the tree species, time lags were calculated. Time lags between changes in environmental parameters and changes in  $Q_s$  at the stem base are indicators for the stem water capacitance of a tree (Čermák et al., 2007). For calculating the time lag between changes in  $D$  or  $E$  (the variables driving evaporation) and changes in  $Q_s$ , cross correlation was applied. The calculated  $Q_s$  signals for each tree for the whole measurement period were compared with the environmental parameters  $D$  and  $E$ . Cross correlation analysis takes two time series signals and calculates the time shift where both signals show the highest similarity. This can be achieved by shifting the two signals step-wise (in this study the steps represent the 15min measurement interval) versus each other and calculating the cross correlation for each step. The time shift where the calculated cross correlation function reaches its maximum marks the highest accordance of the two signals. By taking the mean of these values for each tree species separated by treatment, the time lag can be calculated.

#### **2.6.5 Applied statistical methods**

For the calculation of the correlation between environmental parameters and  $Q_{s-nor}$  simple correlation coefficients were calculated. To further quantify the relationship between environmental parameters and  $Q_{s-nor}$ , linear regression models were performed in R. In a first step, simple models with the relationship between  $Q_{s-nor}$  and one environmental parameter were applied ( $Q_{s-nor} \sim$  environmental parameter). Additionally, additive linear models were calculated including  $Q_{s-nor}$  and two or three environmental parameters ( $Q_{s-nor} \sim$  environmental parameter + environmental parameter). Cross correlation analysis was applied for the calculation of the time lags of  $Q_s$  and environmental parameters (see chapter 2.6.4). To statistically verify differences in observations, ANOVA tests were performed.

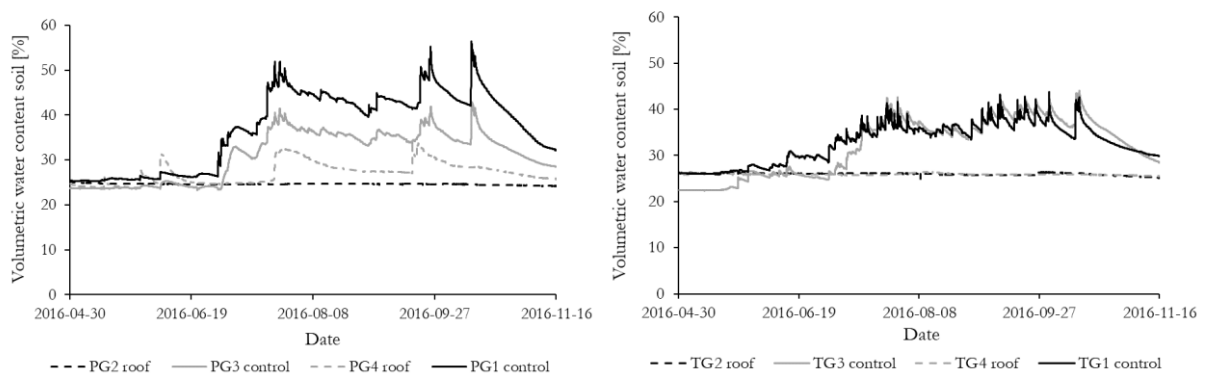


### 3 Results

#### 3.1 Soil water content

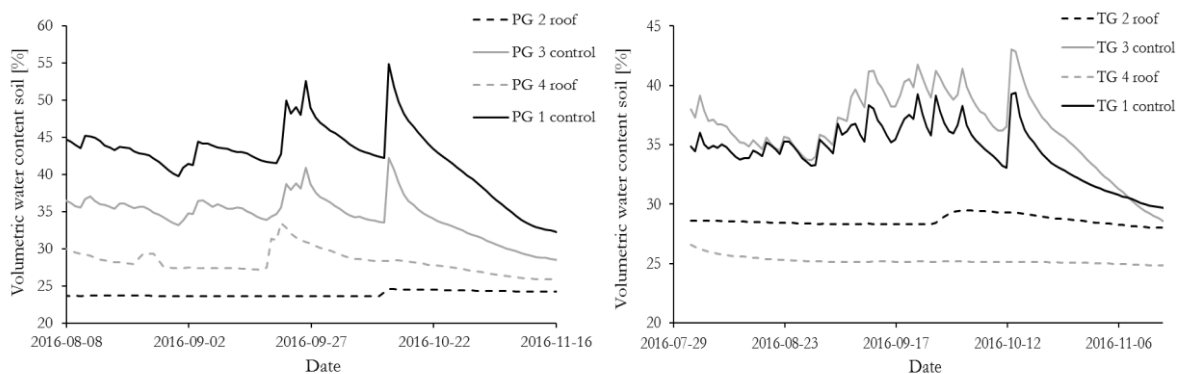
For the comparison of the SWC<sub>v</sub> data amongst the plots, all sensors until a depth of 50 cm were selected and the mean value was calculated for that section of the soil. As mentioned in chapter 2.3, SWC<sub>v</sub> was measured at each plot in varying depth in Tashigang Goempa. An overview about the distribution of the SWC<sub>v</sub> sensors is given in Table 4.

The mean of SWC<sub>v</sub> measured in the first 50 cm from May 2016 until the mid of November 2016 are given in Figure 22.



**Figure 22:** Mean volumetric water content per plot in Pangsho Goempa (broadleaf forest - left) and for Tashigang Goempa (mixed conifer forest – right) for measurements until 50 cm depth from May until November 2016.

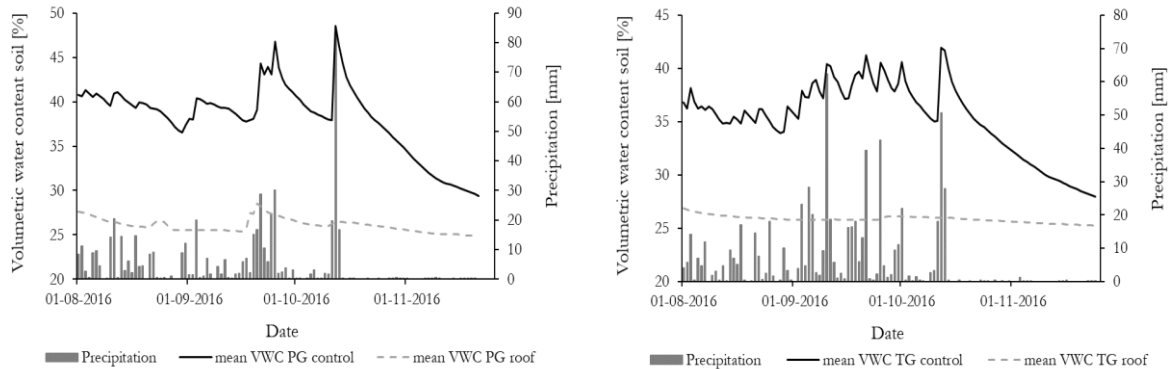
In May 2016, before the start of the monsoon season, SWC<sub>v</sub> differed only little between the control and treatment plots on both sites. Values were around 25 % volumetric water content for all plots. By the end of May, precipitation was getting more frequent and SWC<sub>v</sub> increased for the control plots. To get a more detailed view on the results, Figure 23 is showing the volumetric water content values only for the time period where the sap flow measurements were analysed for this study.



**Figure 23:** Mean volumetric water content per plot in Pangsho Goempa (PG, broadleaf forest - left) and for Tashigang Goempa (TG, mixed conifer forest – right) for measurements until 50 cm depth during the measurement period.

Values for the treatment plots are at both sites lower than for the control plots. At the broadleaf forest site, it appears, that the roof or/and trenches at plot PG4 are not working as good as at the other treatment plots. There are still clear increases in SWC<sub>v</sub> observable indicating a less effective through-fall exclusion.

Values for SWC<sub>v</sub> vary more amongst the plots in the broadleaf forest compared to the plots at the mixed coniferous forest, where values among the plots with same treatment are more homogeneous. Still, it has to be considered, that each plot only contains one soil profile with SWC<sub>v</sub> sensors and therefore can be affected by small variations on this particular spot.



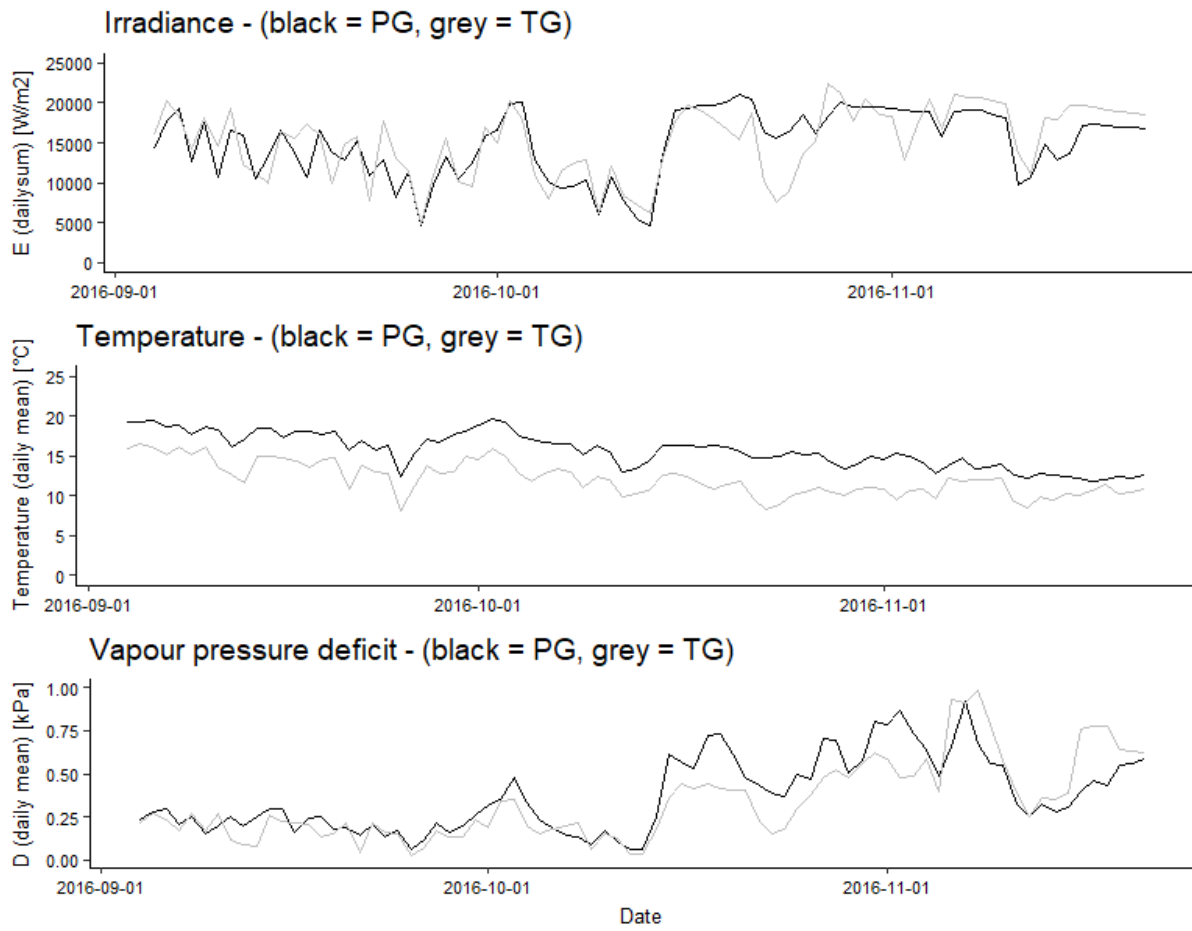
**Figure 24: Mean volumetric water content per site and treatment in relationship to precipitation (Tashigang Goempa - right, Pangsho Goempa - left).**

Figure 24 shows the mean values for the plots with same treatment in comparison to the precipitation measured by the weather stations at each site. From August until mid of October precipitation was frequent and high on both sites. After mid of October the monsoon stopped and the dry period started with only very little recorded precipitation.

There is a clear effect of the through-fall exclusion-roofs visible in SWC<sub>v</sub> of at least 10 to 15% between the treatment and control plots. This difference got smaller once the dry period started (mid of October), when also the control plots were receiving less precipitation, causing a slow drying out of these soils as well.

### 3.2 Weather data

Figure 25 shows the relevant meteorological parameters measured by the weather stations described in chapter 2.2. For the broadleaf forest (PG) higher mean temperatures can be observed over the measurement period. Total *E* was higher at the mixed coniferous site. After the end of the monsoon period in mid of October, *E* was more stable and also *D* increased over the course of the measurement period on both sites.



**Figure 25: Climate data at the broadleaf forest (PG) and mixed conifer forest (TG).**

The correlation matrices in Figure 26 and Figure 27 show the correlation coefficients for the daily mean values of the environmental parameters  $E$ , temperature,  $D$  and SWC<sub>v</sub> for both sites. Strong positive correlations can be observed for SWC<sub>v</sub> between control and roof plots at both sites with higher values for Tashigang Goempa ( $r = 0.83$ ) compared to Pangsho Goempa ( $r = 0.74$ ).  $D$  strongly correlates with  $E$  on both sites ( $r = 0.76$  in Tashigang Goempa,  $r = 0.82$  in Pangsho Goempa). The negative correlation of  $D$  with SWC<sub>v</sub> is stronger at the Tashigang Goempa site ( $r = -0.77$  at control and  $r = -0.70$  at roof plot) compared to the Pangsho Goempa site ( $r = -0.52$  at control and  $r = -0.41$  at roof plot).

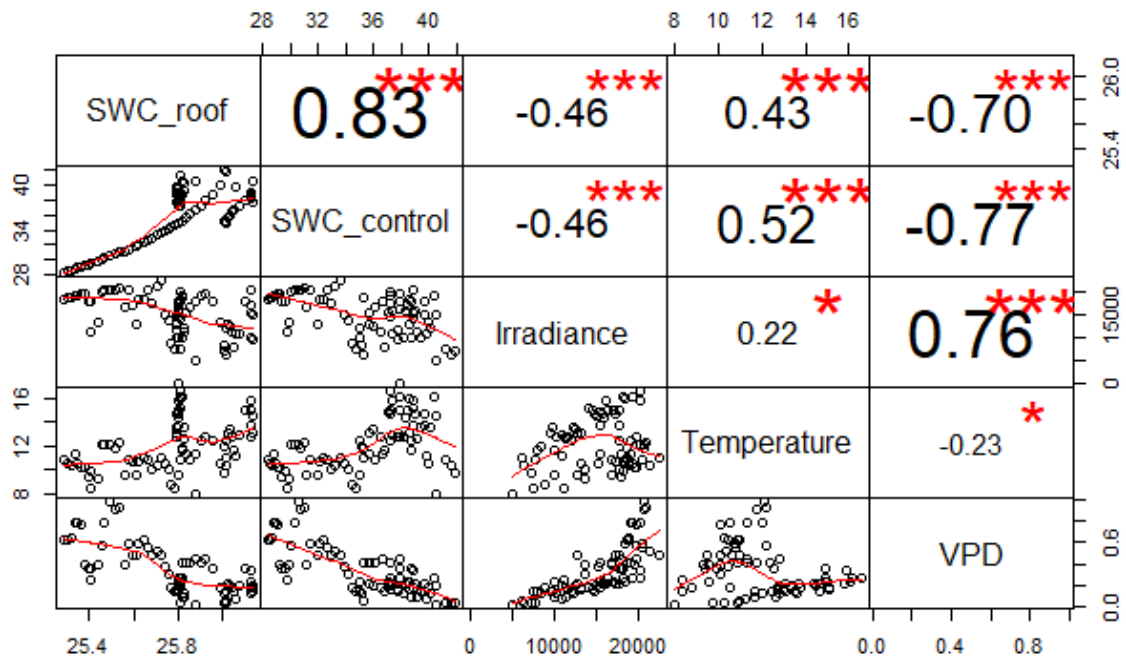


Figure 26: Correlation matrix of daily means/sums of climatic variables at Tashigang Goempa (mixed coniferous forest).

(VPD = Vapour pressure deficit)

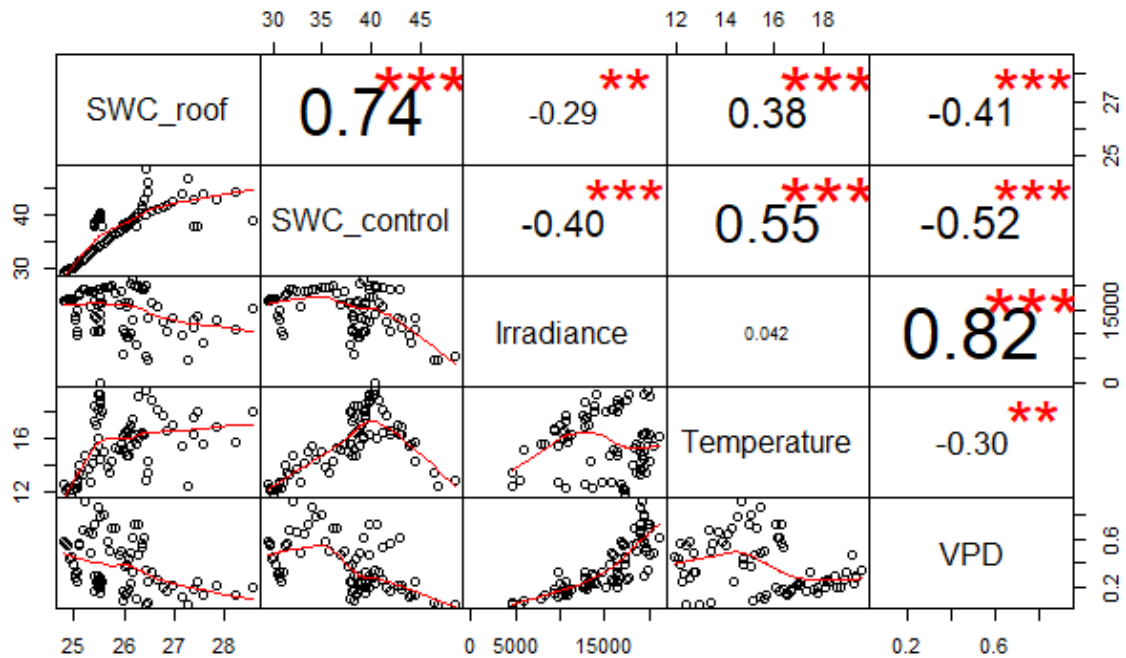


Figure 27: Correlation matrix of daily means/sums of climatic variables at Pangsho Goempa (broadleaf forest).

(VPD = Vapour pressure deficit)

### 3.3 Sap flow data

Data for sap flow is available for most days from 4<sup>th</sup> of September 2016 until 21<sup>st</sup> of November 2016. Periods with poor signal (see chapter 2.6.1) were eliminated although this only occurred in few occasions during the measurement period. The number of individuals with sap flow sensors, separated by species and treatment is shown in Table 5. Only one individual each of *Quercus lanata* and *Rhododendron arboreum* at the broadleaf forest site are not included in the evaluation of sap flow as they both only delivered poor signals during the measurement period.

Figure 28 shows the comparison of control and roof plots for the mean daily sap flow density ( $Q_{s-sum}$ ) for each species of the trial. The grey error bars represent the standard deviation within the species. It is assumed, that because of the high variability in  $Q_{s-sum}$  within some of the species, the differences in  $Q_{s-sum}$  between roof and control plots sometimes do not appear clearly.

During monsoon time (September until mid of October) only for *Rhododendron arboreum* on both sites, and *Quercus semecarpifolia* in the mixed coniferous site, a difference between control and treatment plots is visible. When having a look at the p-values from t-tests performed for each day to see the difference between control and roof plots (Figure 29), there is no result available for this period for *Rhododendron arboreum* and *Quercus semecarpifolia*. This is caused by the low number of trees with good signals available during that time. Therefore, it cannot be concluded that there is a significant difference between control and treatment plots for these two species. Also signals for *Rhododendron arboreum* species are varying heavily or were mostly very low during that time.

For *Quercus lanata* no difference between treatment and control is visible during the whole measurement period and standard deviation within the species is high. Also, the p-values for *Quercus lanata* in Figure 29 do not show significant differences throughout the measurement period. *Quercus griffithi* and *Tsuga dumosa* are showing no differences in  $Q_{s-sum}$  during monsoon but differ significantly after mid of October (Figure 28, Figure 29).

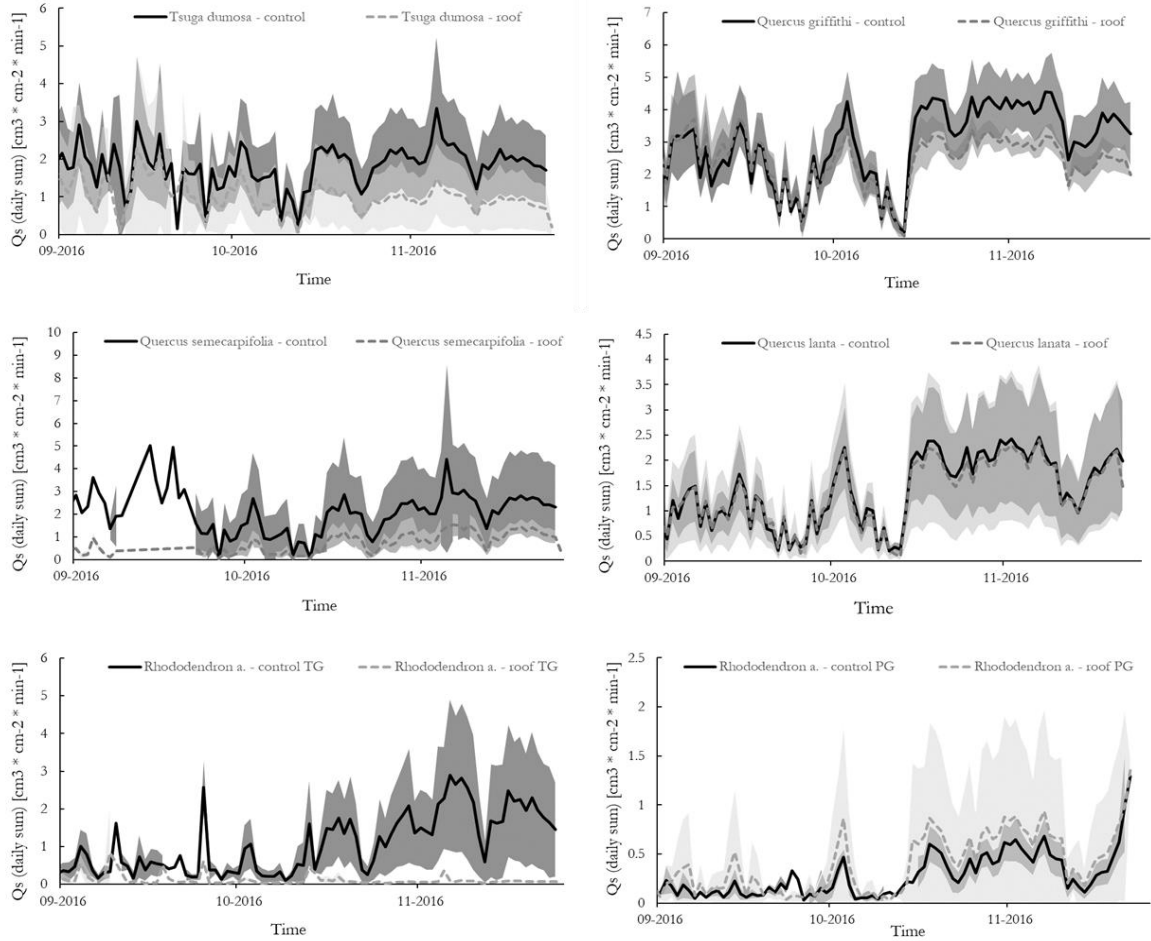


Figure 28: Mean daily sap flow density per species and treatment. The shaded grey areas represent the standard deviation within the species (dark grey = SD control, bright grey = SD treatment).

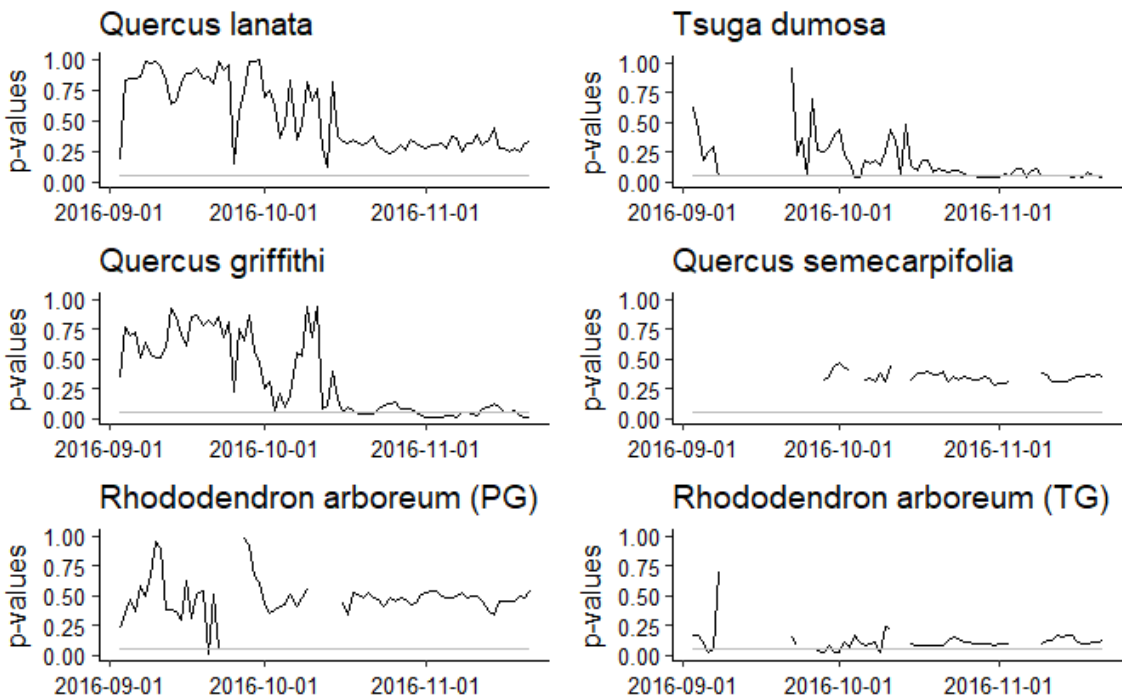
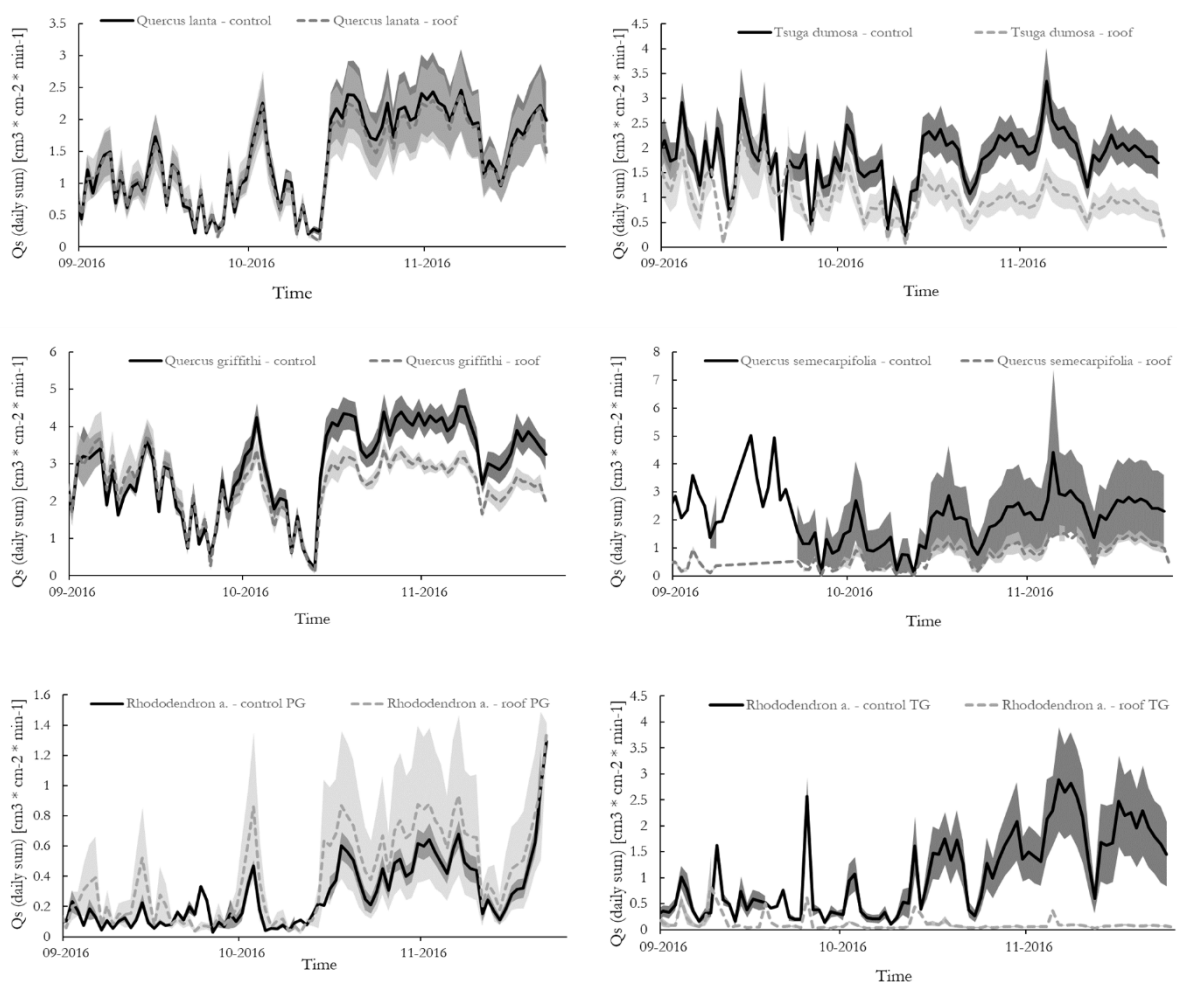


Figure 29: Comparison of p-values from t-test to evaluate differences between control and roof plots over time (the grey line represents the 0.05 significance level).

The standard error of the results for  $Q_{s\text{-sum}}$  (Figure 30) provides further details. Due to the higher number of measured individuals and the lower standard deviation, the standard errors for *Quercus griffithi* and *Tsuga dumosa* are low. Although the same number of individuals of *Quercus lanata* ( $n=10$ ) and *Quercus griffithi* ( $n=10$ ) were equipped with sensors, the standard errors for *Quercus lanata* are much higher. The high intra-specific fluctuation might also be the cause that the mean values for all trees do not show any differences when compared with individuals at control and roof plots. Especially one tree (#128) showed much higher sap flow density values though it is situated on a roof plot. The highest values of sap flow density during midday were sometimes double as high as the highest sap flow signals from the control plot (Figure 31).

There were only five trees of *Quercus semecarpifolia* included in the study. This causes high standard errors for the trees at the control plot where only two individuals are represented. Also for *Rhododendron arboreum* the variation of the  $Q_{s\text{-sum}}$  at the treatment plots at Pangsho Goempa and at the control plots at Tashigang Goempa are very high.



**Figure 30: Mean daily sap flow density per species and treatment. The shaded grey areas are representing the standard error within the species (dark grey = SE control, bright grey = SE treatment).**

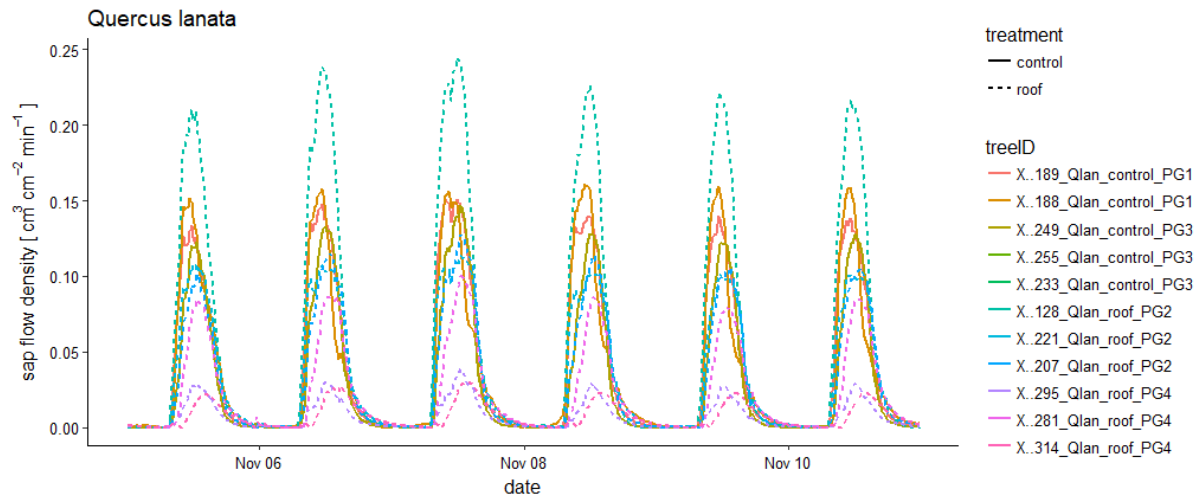


Figure 31: Sap flow density of single trees for *Quercus lanata* on six days in November 2016.

### 3.3.1 Correlation of $Q_{s-nor}$ with environmental factors

As sap flow strongly depends on environmental factors, the correlation between  $Q_{s-nor}$  and  $D$ ,  $E$  and  $SWC_v$  was tested. The results of the Pearson correlation tests including significance levels are given in Table 7.

Table 7: Pearson correlation coefficients and significance levels for climatic variables and standardized sap flow density separated by treatment (control/roof).

Species	$D$		$E$		$SWC_v$	
	control	roof	control	roof	control	roof
<i>Tsuga dumosa</i>	0.633 ***	0.366 **	0.842 ***	0.686 ***	-0.33 **	-0.1
<i>Quercus semecarpifolia</i>	0.873 ***	0.933 ***	0.837 ***	0.79 ***	-0.67 ***	-0.69 ***
<i>Rhododendron a. (TG)</i>	0.783 ***	0.865 ***	0.557 ***	0.689 ***	-0.58 ***	-0.69 ***
<i>Quercus griffithi</i>	0.884 ***	0.613 ***	0.82 ***	0.861 ***	-0.54 ***	-0.35 **
<i>Quercus lanata</i>	0.942 ***	0.944 ***	0.911 ***	0.902 ***	-0.55 ***	-0.41 ***
<i>Rhododendron a. (PG)</i>	0.588 ***	0.944 ***	0.436 ***	0.776 ***	-0.12	-0.26 *

Significance codes: \*\*\* :  $p < 0.001$ , \*\* :  $p < 0.01$ , \* :  $p < 0.05$

#### 3.3.1.1 Correlation of $Q_{s-nor}$ and $D$

The correlation between  $Q_{s-nor}$  and  $D$  is given in the graphs in Figure 32. All tree species show a positive correlation with increasing  $D$ . All tree species except *Rhododendron arboreum* are showing a saturation effect with less increase in  $Q_{s-nor}$  at higher  $D$  values.



As described in chapter 2.6.3 the calculation of  $Q_{s-nor}$  eliminates the differences in absolute sap flow density. To see a difference between trees at the control and roof plots, the trees would have to show a difference in the correlation pattern which cannot be observed for all tree species. ANCOVA-tests to examine the effect of the treatment were only showing significant differences for *Quercus griffithi*, *Quercus semecarpifolia* and *Rhododendron arboreum* (at the broadleaf forest). For *Tsuga dumosa* and *Quercus griffithi* some trees on the treatment plots show very high  $Q_{s-nor}$  at low  $D$ .

**Table 8: p-values of ANCOVA-test for treatment effect in correlation of  $Q_{s-nor}$  and  $D$**

Species	p-values ANCOVA ( $Q_{s-nor} \sim D * \text{treatment}$ )
<i>Tsuga dumosa</i>	0.904
<i>Quercus semecarpifolia</i>	9.88e-11 ***
<i>Rhododendron a. (TG)</i>	0.107
<i>Quercus griffithi</i>	1.58e-14 ***
<i>Quercus lanata</i>	0.410
<i>Rhododendron a. (PG)</i>	0.018 *

Significance codes: \*\*\* :  $p < 0.001$ , \*\* :  $p < 0.01$ , \* :  $p < 0.05$

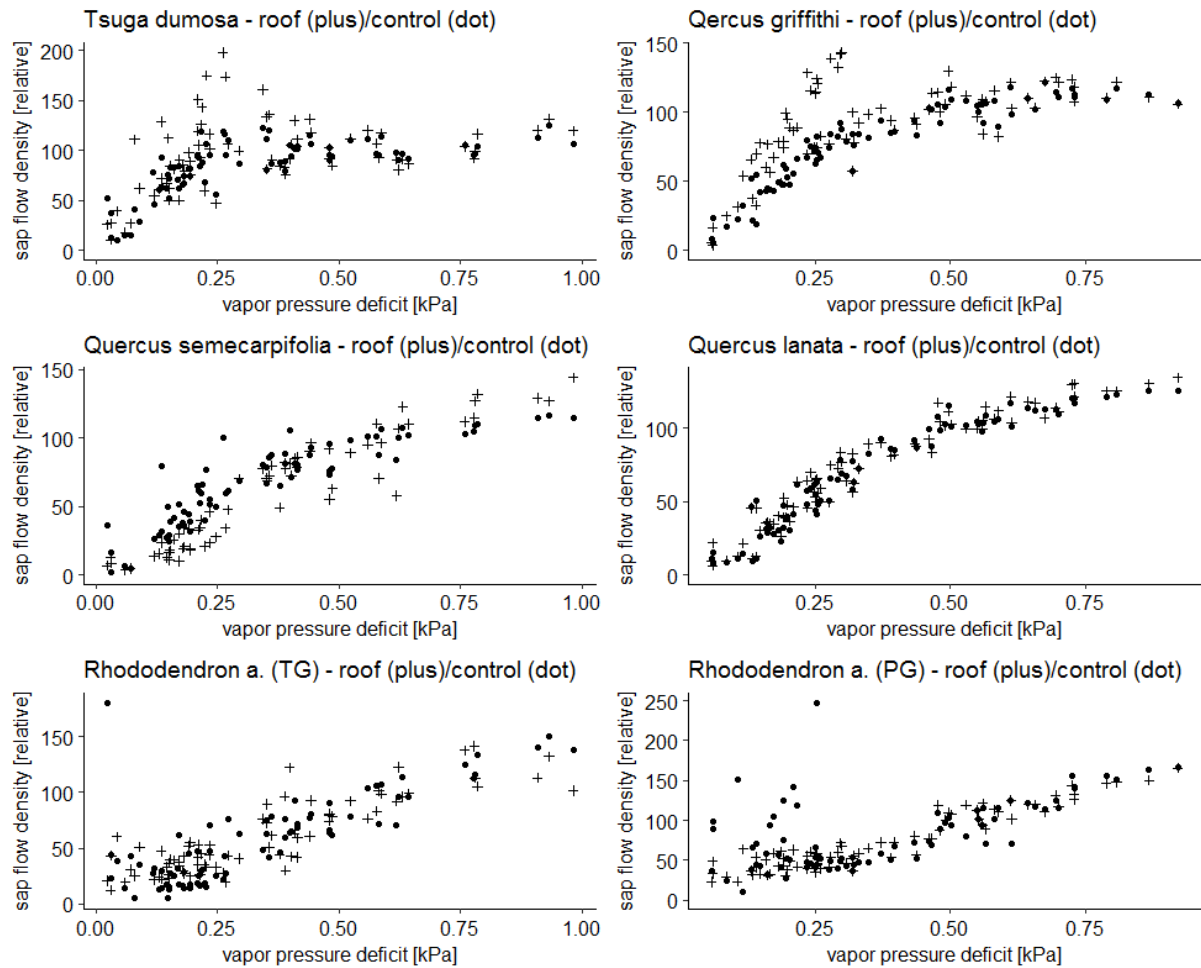


Figure 32: Correlation of  $Q_{s-nor}$  (=relative sap flow density) and  $D$  per tree species.

### 3.3.1.2 Correlation of $Q_{s-nor}$ and $E$

The correlation plots of  $Q_{s-nor}$  and  $E$  are showing a similar pattern as the correlation of  $Q_{s-nor}$  and  $D$ . There is positive correlation with increasing  $E$  which was measured in all trees. In contrast to the correlation with  $D$ ,  $Q_{s-nor}$  increases linearly with  $E$  without reaching an apparent saturation. ANCOVA-tests to examine the effect of the treatment (Table 9) were only showing significant differences for *Quercus griffithi* and *Quercus semecarpifolia*.

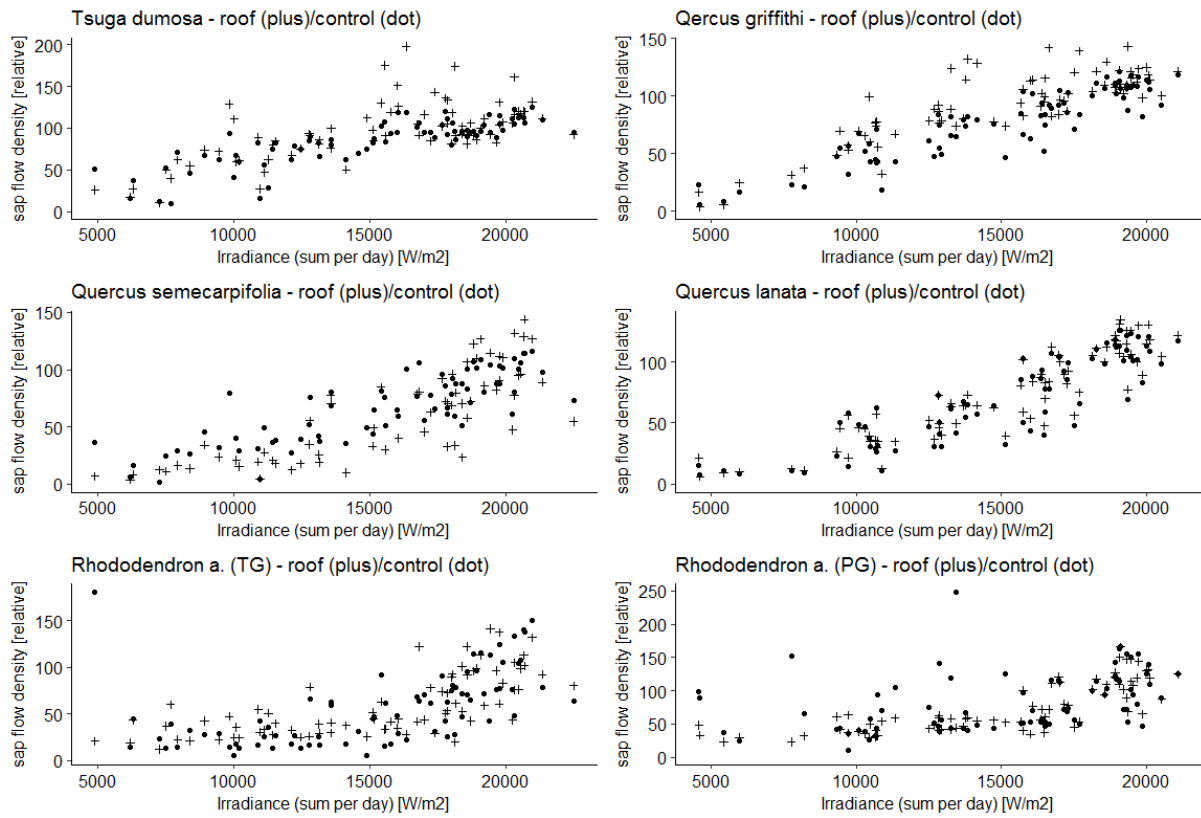


Figure 33: Correlation of  $Q_{s-nor}$  (=relative sap flow density) and  $E$  per tree species.

Table 9: : p-values of ANCOVA-test for treatment effect in correlation of  $Q_{s-nor}$  and  $E$

Species	p-values ANCOVA ( $Q_{s-nor} \sim E * \text{treatment}$ )
<i>Tsuga dumosa</i>	0.587
<i>Quercus semecarpifolia</i>	0.021 *
<i>Rhododendron a. (TG)</i>	0.573
<i>Quercus griffithi</i>	1.83e-05 ***
<i>Quercus lanata</i>	0.807
<i>Rhododendron a. (PG)</i>	0.157

Significance codes: \*\*\* :  $p < 0.001$ , \*\* :  $p < 0.01$ , \* :  $p < 0.05$

### 3.3.1.3 Correlation of $Q_{s-nor}$ and SWCv

The correlation plots of  $Q_{s-nor}$  and SWCv show a negative correlation with increasing SWCv. There is a clear distinction between the roof and control plots as SWCv is lower on the roof plots. SWCv on the control plots varies stronger than on the roofed plots which can be seen more clearly in

In May 2016, before the start of the monsoon season, SWCv differed only little between the control and treatment plots on both sites. Values were around 25 % volumetric water content for all plots. By the end of May, precipitation was getting more frequent and SWCv increased for the control plots. To get a more

detailed view on the results, Fig. 23 shows the volumetric water content values only for the time period where the sap flow measurements were analysed for this study.

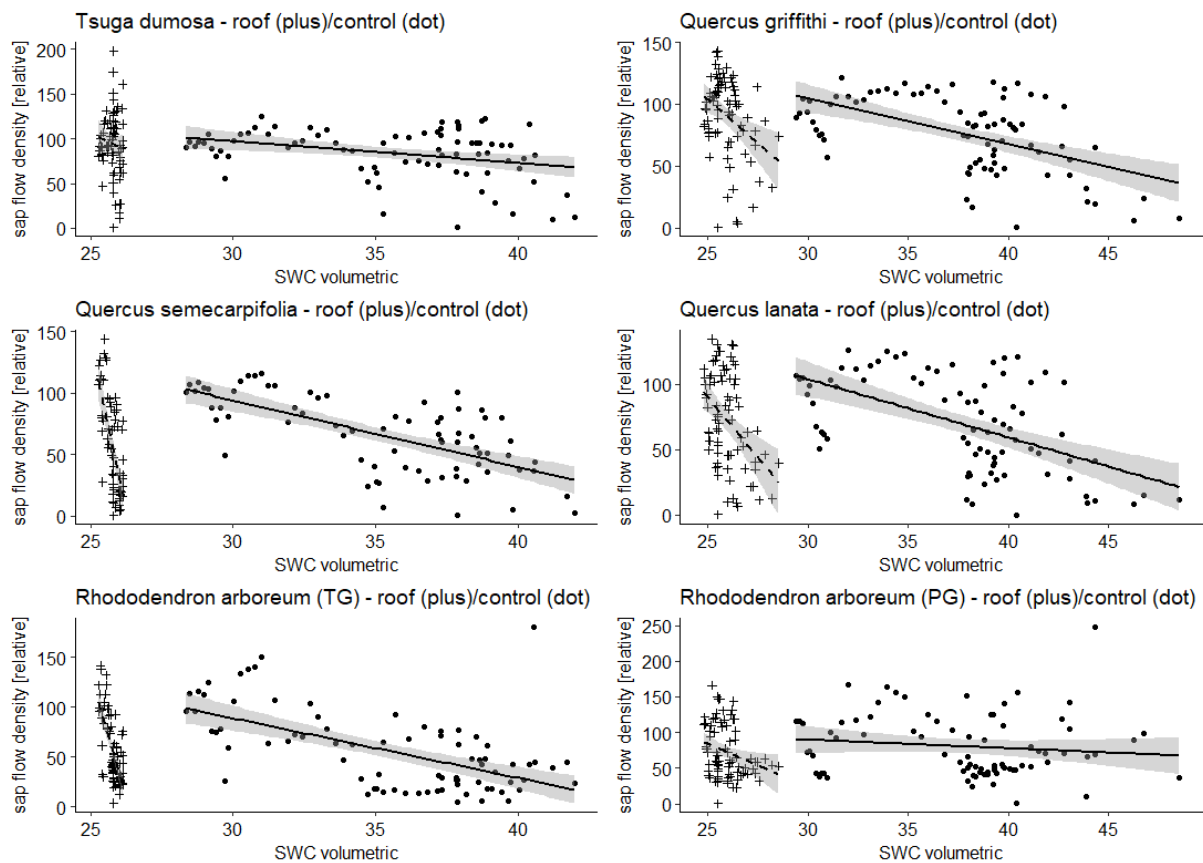


Figure 34: Correlation of  $Q_{s-nor}$  (=relative sap flow density) and SWCv per tree species.

### 3.3.2 Linear regression models for sap flow and environmental factors

The results of the linear regression for all three environmental factors are given in Table 10. Estimates, R-squared values and significance levels are provided for all tree species separated by treatment. *Quercus* species show generally high R-squared values for *D* and *E*. The correlation factors for SWCv is generally low with values below 0.5 for all species. *Tsuga dumosa* trees under roof show a very low R-squared with 0.12 compared to 0.39 in the control area.

Estimates for SWCv are negative for all tree species. Further regression models with additive model approaches including *E* and SWCv as well as *D* only added small improvements to the model but did not explain the negative estimates for SWCv.

Table 10: Estimates and R<sup>2</sup> values from linear regression for climatic variables and Q<sub>s-nor</sub> separated by treatment (control/roof).

Species	<i>D</i>						<i>E</i>						SWC <sub>v</sub>					
	control			roof			control			roof			control			roof		
	Estimate		R <sup>2</sup>	Estimate		R <sup>2</sup>	Estimate		R <sup>2</sup>	Estimate		R <sup>2</sup>	Estimate		R <sup>2</sup>	Estimate		R <sup>2</sup>
<i>Tsuga dumosa</i>	73.55	***	0.39	56.54	***	0.12	0.0049	***	0.67	0.0052	***	0.42	-2.43	**	0.10	-15.36		0.00
<i>Quercus semecarpifolia</i>	114.07	***	0.76	156.6	***	0.87	0.0056	***	0.68	0.0068	***	0.62	-5.41	***	0.44	-108.39	***	0.47
<i>Rhododendron a. (TG)</i>	123.46	***	0.61	123.46	***	0.74	0.0048	***	0.29	0.0050	***	0.45	-5.99	***	0.33	-97.73	***	0.47
<i>Quercus griffithi</i>	122.06	***	0.78	87.23	***	0.37	0.0064	***	0.82	0.0061	***	0.71	-3.70	***	0.28	-14.10	**	0.11
<i>Quercus lanata</i>	156.62	***	0.89	155.83	***	0.89	0.0075	***	0.77	0.0076	***	0.82	-4.46	***	0.29	-18.46	***	0.16
<i>Rhododendron a. (PG)</i>	116.62	***	0.34	161.03	***	0.89	0.0040	***	0.15	0.0067	***	0.58	-1.20		0.00	-12.16	*	0.06

Significance codes: \*\*\* : p < 0.001, \*\* : p < 0.01, \* : p < 0.05

### 3.3.3 Time lag of $Q_s$ and environmental factors

A further characterisation method for different tree species on how their water transport is influenced by short-term changes in their environment is their response to varying climatic factors. The time lag between changes in  $D$  or  $E$  and the measured  $Q_s$  at the base of the stem reflects the water capacitance of the tree stem. By performing a cross correlation between these two environmental variables and measured  $Q_s$  results in the time lag for each species.

#### 3.3.3.1 Cross correlation and time lag of $Q_s$ and vapour pressure deficit

The results for the time lag of  $Q_s$  to  $D$  are given in Figure 35. The combined effect of species and treatment shows no significance ( $p = 0.1993$ ) when running a ANOVA-test. An ANOVA analysis of the time lags showed significant differences between the species ( $p$ -value:  $9.83E-10$ ).

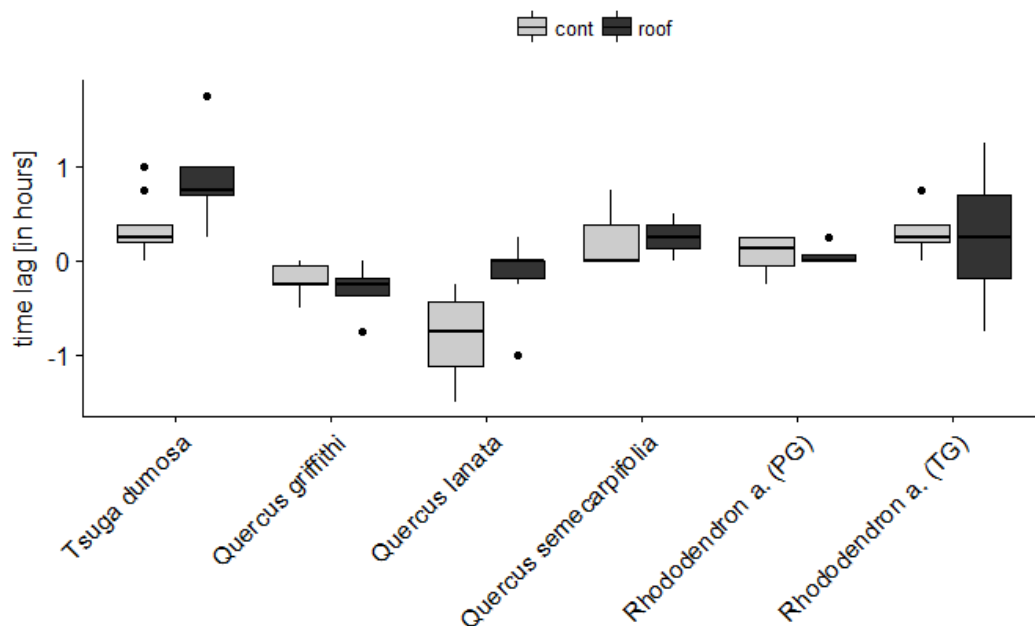


Figure 35: Time lags of  $Q_s$  to  $D$  of different tree species distinguished by treatment.

The box plot also provides information on the variation of the cross-correlation for the individual trees within a tree species. *Quercus lanata* and *Quercus griffithii* (both at the Pangsho Goempa site) show the shortest time lag. *Quercus semecarpifolia* and *Rhododendron arboreum* trees show a time lag of 45 min to 60 min until changes in  $D$  can be mostly observed in their  $Q_s$  signal. The mean time lag is longest for *Tsuga dumosa* trees with a mean value of more than 75 minutes.

When having a look at the effect of the roof on the time lag of the different tree species, only small variations can be observed. Only for *Quercus lanata* and *Tsuga dumosa*, larger differences in the time lag between control and treatment trees can be observed, which are significant only for *Tsuga dumosa*.

**Table 11: Statistical summary for ANOVA-analysis testing the differences in lags (from  $D$ ) by treatment.**

Tree species	F-value	p-values	sign. Level	mean control	mean roof
<i>Tsuga dumosa</i>	6.26	0.025	*	1.3	3.3
<i>Quercus lanata</i>	4.26	0.073		-3.2	-0.7
<i>Quercus semecarpifolia</i>	0	1		1	1
<i>Rhododendron arboreum</i> (PG)	0	1		0.3	0.3
<i>Rhododendron arboreum</i> (TG)	0.02	0.894		1.3	1
<i>Quercus griffithi</i>	0.44	0.526		-0.8	-1.3

Significance codes: \*\*\*:  $p < 0.001$ , \*\*:  $p < 0.01$ , \*:  $p < 0.05$

Figure 36 additionally contains the diurnal patterns for  $D$  of a *Quercus lanata* and a *Quercus griffithi* tree at the broadleaf forest site. On this clear sky day  $Q_s$  and  $D$  start to rise as soon as temperature rises.  $Q_s$  for both trees reaches its daily maximum earlier compared to  $D$  explaining the negative time lags in Figure 35.

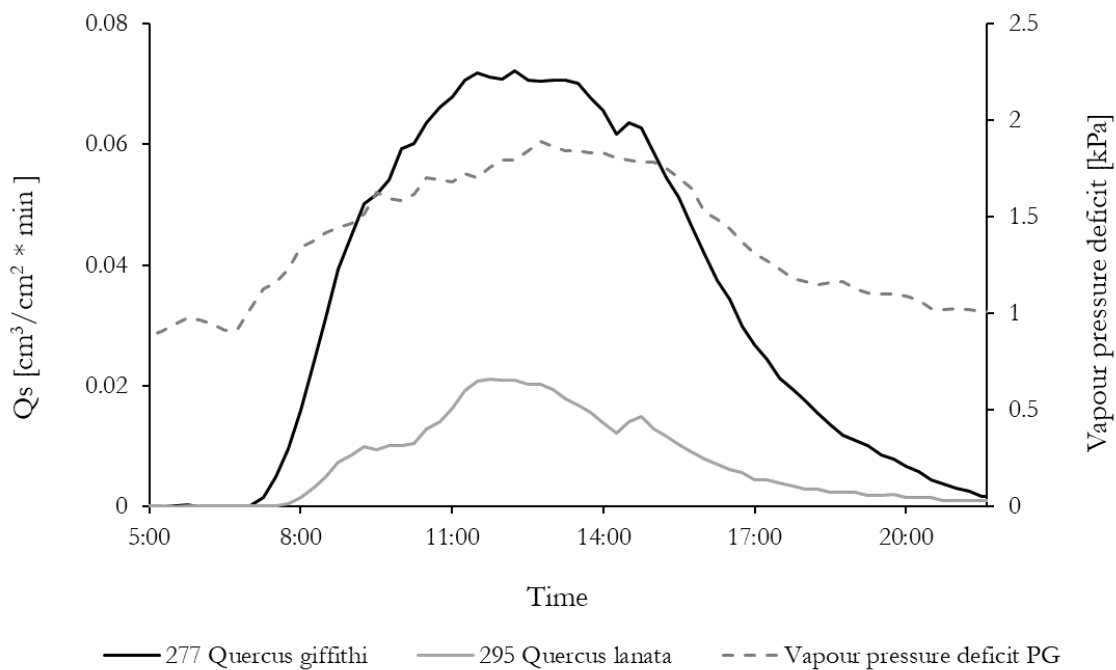


**Figure 36: Diurnal pattern of  $Q_s$  and  $D$  for a day in November 2016**

Further illustrations on the diurnal pattern of  $Q_s$  for the different species in relationship to  $D$  are shown in Figure 37 and Figure 38. The maximum values for each day and tree were taken and the relative values were calculated for all 15-min-values of this day. The comparison of these results provides a better overview about the response of the different tree species to  $D$ .

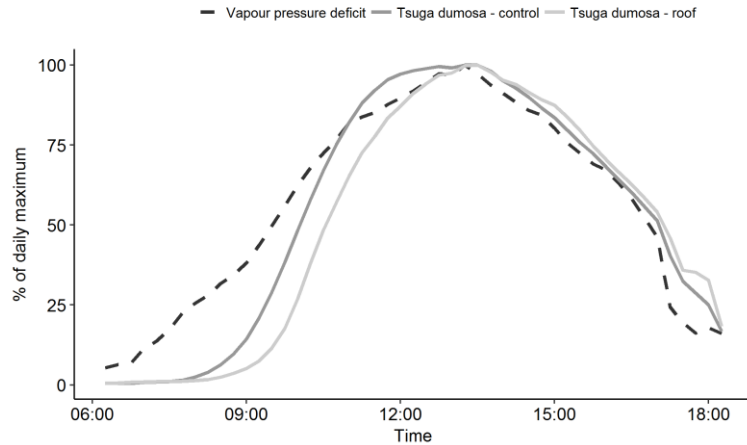


Figure 37: Diurnal shape of  $Q_s$  in % of the daily maximum value for the whole measurement period in comparison to  $D$  for *Tsuga dumosa*.

Figure 37 shows the time lag for *Tsuga dumosa* to  $D$  on the mixed conifer forest site separated by treatment.  $D$  starts to rise at 6:30 in the morning whereas changes in  $Q_s$  only start at 08:00 for control trees and at 08:30 for the trees under the roof.  $Q_s$  rapidly increases in the morning compared to  $D$  so that all three parameters are reaching their maximum at 13:00. In the afternoon  $Q_s$  and  $D$  decline synchronously.

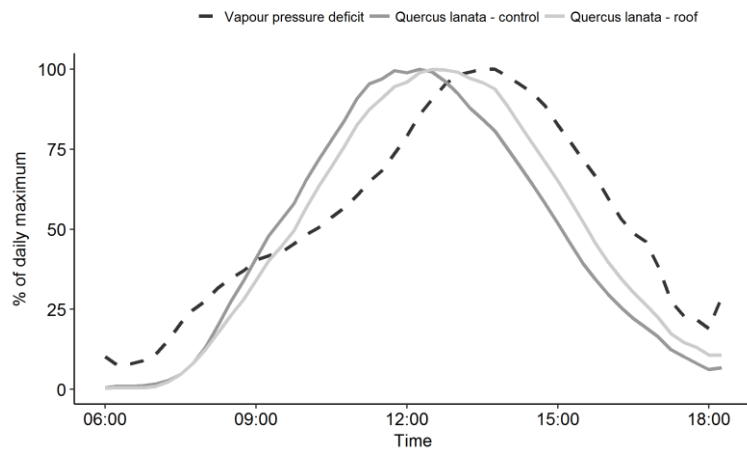


Figure 38: Diurnal shape of  $Q_s$  in % of the daily maximum value for the whole measurement period in comparison to  $D$  for *Quercus lanata*.

*Quercus lanata* on the broadleaf forest site is showing a different behaviour. Though changes in  $Q_s$  start again later than  $D$ , both curves for  $Q_s$  (control and roof plot) are reaching their maximum before  $D$  is at maximum. In contrast to *Tsuga dumosa*, both  $Q_s$  curves also decline faster after midday compared to the  $D$ . The whole pattern finally explains the negative time lags shown in Figure 35.



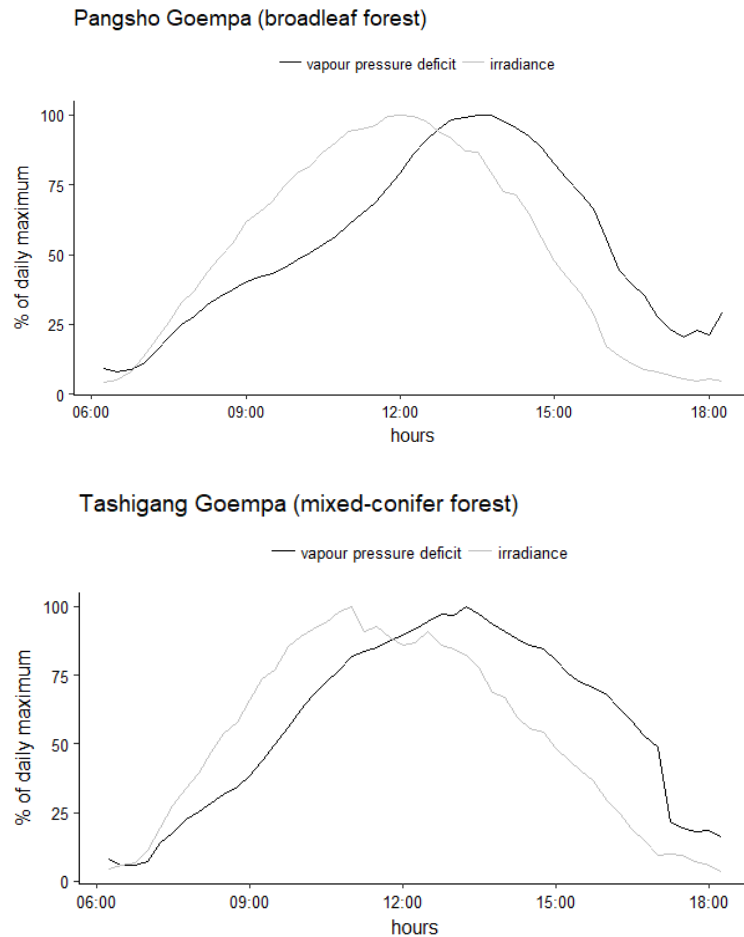
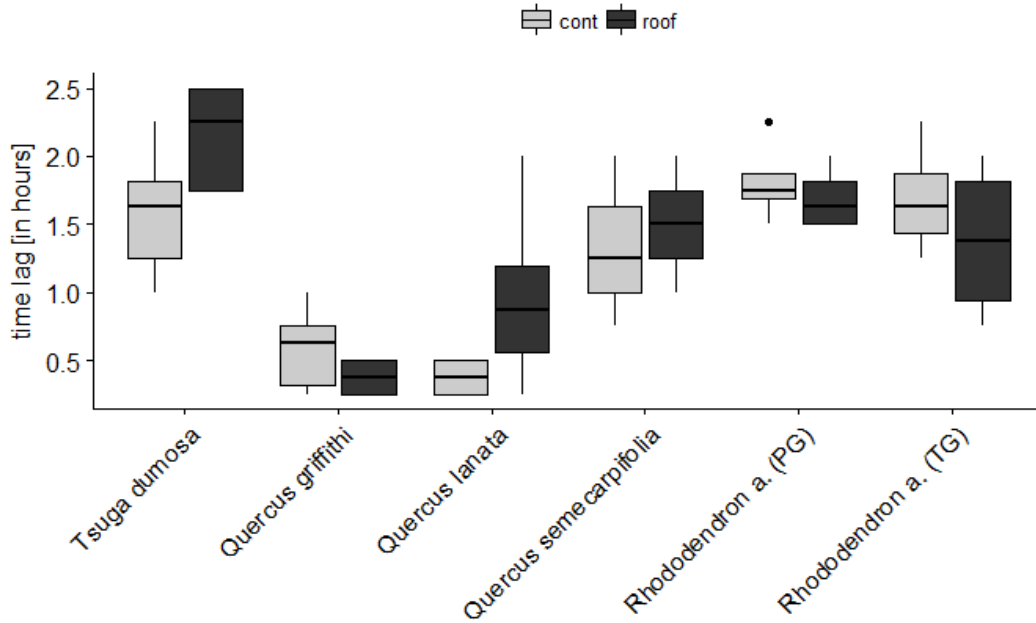


Figure 39: Comparison of mean diurnal course of vapour pressure deficit and irradiance for both sites (in % of daily maximum).

The mean diurnal courses of irradiance and vapour pressure deficit for both sites of the present study are shown in Figure 39. At both sites, vapour pressure deficit had a time lag to irradiance.

### 3.3.3.2 Cross correlation and time lag of $Q_s$ and $E$

The results for the relationship of  $Q_s$  and  $E$  are very similar to the results of  $Q_s$  and  $D$ . As can be seen in Figure 40. Fehler! Verweisquelle konnte nicht gefunden werden. *Tsuga dumosa* shows again the highest values for time lags and *Quercus griffithii* and *Quercus lanata* have the lowest values.



**Figure 40:** Time lags of  $Q_s$  to  $E$  for different tree species distinguished by treatment.

In general, all time-lag-values for  $Q_s$  and  $E$  for each species are higher compared to the time lag  $Q_s$  and  $D$ . The combined effect of species and treatment shows only low significance ( $p = 0.0642$ ) when running a ANOVA-test. The differences between the species are again significant according to ANOVA analysis ( $p = 5.69E-06$ ).

Similar to the results for the relationship of  $Q_s$  and  $D$ , there is no difference in the time lag, between individuals on the control and the roof plot. The results from the ANOVA-test only show differences between treatments for *Tsuga dumosa* trees. As can be seen in Table 12, there was no significant difference visible for the other tree species.

**Table 12:** Statistical summary for ANOVA-analysis testing the differences in lags (from  $E$ ) by treatment.

Tree species	F-value	p-values	sign. Level	mean control	mean roof
<i>Tsuga dumosa</i>	8.40	0.012	*	6.4	8.6
<i>Quercus lanata</i>	3.28	0.108		1.5	3.8
<i>Quercus semecarpifolia</i>	0.08	0.799		5.3	6.0
<i>Rhododendron arboreum</i> (PG)	0.40	0.550		7.3	6.8
<i>Rhododendron arboreum</i> (TG)	0.73	0.426		6.8	5.5
<i>Quercus griffithi</i>	1.60	0.242		2.3	1.5

Significance codes: \*\*\*:  $p < 0.001$ , \*\*:  $p < 0.01$ , \*:  $p < 0.05$

Analysing the shape of the diurnal pattern of  $E$  and  $Q_s$  as in Figure 41 and Figure 42 provides a better understanding on how the trees are behaving. In Figure 41 changes in  $E$  are observable at 06:15.  $Q_s$  changes for *Tsuga dumosa* only start at 08:15 (for the control plot) and at 08:45 (for the roof plot).  $E$  reaches its maximum already at 11:00 which might be caused by increasing cloud formation over the course of the day. However,  $Q_s$  reaches its maximum later at 13:00, resulting in a longer time lag between  $Q_s$  and  $E$ .

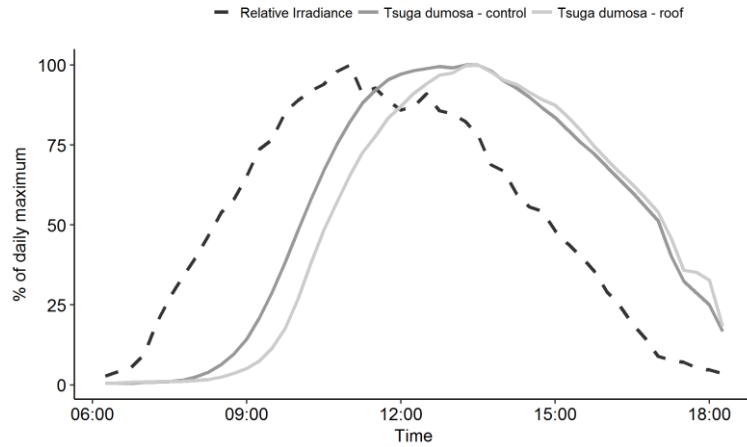


Figure 41: Diurnal shape of sap flow density in % of the daily maximum value for the whole measurement period in comparison to  $E$  for *Tsuga dumosa*

$E$  and  $Q_s$  for *Quercus lanata* at the broadleaf forest site are showing a more synchronous behaviour.  $Q_s$  starts again later in the morning but is showing a faster increase compared to  $E$ . Similar to *Tsuga dumosa*, the trees on the roof plots show a slower response to the irradiance signal, but this cannot be observed for all tree species as can be seen in Figure 40.

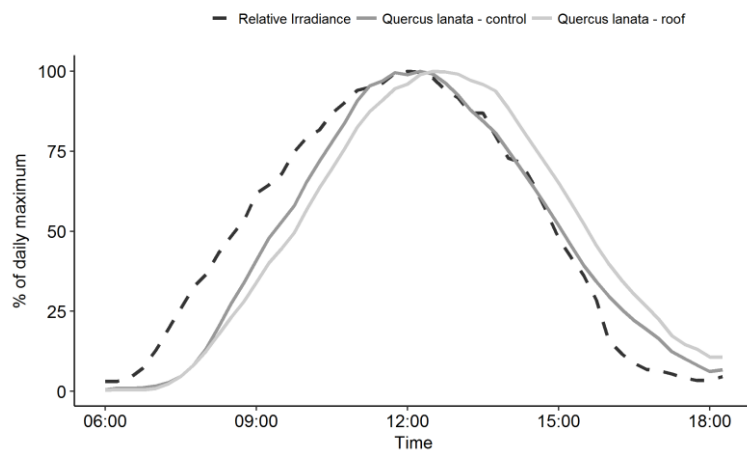


Figure 42: Diurnal shape of  $Q_s$  in % of the daily maximum value for the whole measurement period in comparison to  $E$  for *Quercus lanata*.

## 4 Discussion & Conclusion

### 4.1 Experimental design

Due to the experimental design and data availability, there exist some limitations concerning data evaluation and data comparison. Absolute water consumption at the tree or stand level for instance was not calculated. There is no data available about the depth and activity of sapwood of the measured trees and therefore it is not known if the trees use a large or a small proportion of the rainfall or soil water. Studies, aiming to calculate transpiration of trees or stands (Ghimire et al., 2014; Pangle et al., 2015) should include data of xylem depth by sap flow measurements in different depths. As the focus of this study was to compare trees with or without water stress, this was less important and more emphasis was put on relative sap flow density (per sapwood area) without calculating absolute sap flow per tree. This approach was also taken in other studies (Leo et al., 2014; Du et al., 2011; Leuzinger et al., 2007; Dalsgaard et al., 2011).

A partly unknown factor is the water availability on the treatment plots and how efficient the roofs are excluding the trees' access to soil water. Though comprehensive soil moisture measurements in different depths were taken, uncertainty still remains on how much water was available for the trees. Especially in deeper soil horizons and at the edges of the roof construction some water infiltration occurred. According to the soil moisture measurements, the roofs at Pangsho Goempa (broadleaf forest) were not as efficient as the roofs in Tashigang Goempa (mixed conifer forest). At the plots in Pangsho, there was still an increase (although not as strong as on the control plots) in soil moisture visible during, and after a rain event. However, soil moisture in the upper 50 cm at the treatment plots was always lower compared the control plots. To get a clearer picture on how the water availability for trees under the roof is,  $\delta^{18}\text{O}$  analysis can be done as Leo et al. (2014) did in their experiment.

Due to problems with the reliability of the system in the years 2014, 2015 and 2016, largely un-interrupted data were only available for three months period. This time period represents the last weeks of monsoon and the following dry period in 2016. Ideally, a whole year of data should be available and include a period before drought stress was imposed through the rainfall exclusion. This would provide a better understanding on how the roofs affect the water availability of the trees and would allow to perform further modelling and evaluation approaches.

### 4.2 Impact of through-fall exclusion roofs on sap flow density

The effect of the through-fall exclusion roofs on the water transport on trees was shown by comparing the absolute sap flow density of the different tree species. Trees react to drought-stress by closing their stomata which depends on the plants' water potential. Depending on the tree species and the species' strategy (isohydric – anisohydric), the closure of the stomata happens at different stages of plant water potential (Frey et al., 2010). As plant water potential depends on soil moisture it was assumed that the differences in soil moisture on the treatment and control plots are also present in the sap flow signals.

Significant differences with lower sap flow density measured in trees on the roof plots were observed in the signals of *Quercus griffithii*, *Tsuga dumosa* and *Rhododendron arboreum* (at the coniferous forest site) on only few days during the measurement period. Despite very few exceptions, the days with significant differences are occurring in the dry period after monsoon stopped and the evaporative demand was high. No significant differences between trees on the control and roof plots were detected for *Quercus lanata* and *Quercus semecarpifolia*. However, for *Quercus lanata* one tree on a treatment plot showed very high signals that were even much higher than the trees had at the control plot. It seems that probably the sensor was damaged or the position of the sensor on the tree was not perfect. Nevertheless, the tree was not excluded from the study because there was no clear sign of a malfunction of the sensor. *Rhododendron arboreum* at the through-fall exclusion plots at the broadleaf site shows even higher signals than the control plots. Because of the high intra-specific variations in the sap flow density signals of *Quercus lanata* and *Quercus semecarpifolia*, it is difficult to say if this result is due to problems with the measurement system or if there is no difference between the sap flow density signals. Both species show higher standard errors which are caused by the lower number of trees with sensors and the higher intra-specific variations. The signal strength of *Rhododendron arboreum* at both sites were often very low because in both forest types they represent small understorey trees. This could be an explanation for the not expected inverted result for *Rhododendron arboreum* and the broadleaf site. Similar studies found a clear difference between the sap flow density of control and treatment trees (Leo et al., 2014; Pangle et al., 2015).

For *Quercus griffithii*, *Tsuga dumosa* and *Rhododendron arboreum* at the coniferous forest site the difference in sap flow density increased after the end of the monsoon season in mid-October. After this date,  $D$  and  $E$  increased resulting in a higher evaporative demand for the plants. During this dry period, trees on the control plots with sufficient water supply were able to increase their water consumption while trees on the treatment plots could not increase their transpiration in the same way or even had to reduce it.

To improve the results in the future and to avoid large interference of intra-specific variations, a longer measurement period will be beneficial. Using a whole year of measurements (Pangle et al., 2015) and a time period before the installation of the roof as a base for calculating standardized sap flow density values (Leo et al., 2014) would probably provide clearer results for all species. To check the high variance between signals of trees from the same tree species and treatment it would be beneficial to check the sensors for future measurements. Different positions on the tree stem shall be tested and also the functioning of the sensor has to be checked. Due to the extent of the experiment with 60 trees measured at very remote measurements sites, this remains a big challenge for the future.

### **4.3 Impact of main environmental drivers on sap flow**

Vapour pressure deficit ( $D$ ) and irradiance ( $E$ ) both were strongly correlated with normalised sap flow. Similar results were published by Du et al. (2011) and Pataki et al. (2000) and many other authors.

The main influencing factors on sap flow are outlined in chapter 1.2.2.  $D$  is the major physical driver of evaporation and responsible for negative water potentials in the atmosphere.  $E$  has a strong direct effect on the stomatal aperture. Stomata react fast to PAR (photosynthetic active radiation) and open as the leaf is

exposed to light (Shimazaki et al., 2007). Higher values of  $E$  and  $D$  therefore cause high sap flow unless other factors are limiting stomatal conductance (Frey et al., 2010). This is clearly represented in the results in Figure 32 and Figure 33. Factors which would lower the aperture of stomata are high  $\text{CO}_2$  concentrations, darkness and drought stress (Araújo et al., 2011; Arve et al., 2011). An important role in this context plays ABA (abscisic acid) which is formed when a plant experiences drought stress to minimize water loss by transpiration (Shimazaki et al., 2007).

In comparison to the results from Leo et al. (2014), no clear difference between water stressed and control trees in their response to  $D$  and  $E$  is visible. This is due to the calculation of normalised sap flow density values. As the measurement period lasts only from the beginning of September 2016 till the mid of November 2016 the base for the normalisation calculation is the mean of measured sap flow density values over this whole period for every single tree. Ideally, a period before the installation of the roof would be used to standardize sap flow densities (as in Leo et al., 2014) when  $\text{SWC}_v$  was similar between the treatment and control plots. For future monitoring of sap flow in this experiment, measurements should thus start before the treatment (mounting of roofs) to be able to normalise sap flow under the same conditions for control and treatment trees. The relationship between  $D$  and standardised sap flow was significantly affected by treatment only in *Quercus griffithii*. Surprisingly, the trees of *Quercus griffithii* on the treatment showed higher relative sap flow density values compared to those on the control plots (Figure 32, Figure 33). This result appears implausible. The cause for these high values is due to the calculation of relative sap flow. In the case of *Quercus griffithii*, already during monsoon time high values of sap flow density for the trees under the roof were recorded although  $D$  was low. The calculation of relative sap flow finally led to some measurement points with high relative sap flow values at low  $D$ .

The correlation between  $\text{SWC}_v$  and relative sap flow was negative in all species with lower significance levels compared to the correlation of sap flow with  $D$  and  $E$ . If soil water has an effect, one would rather expect sap flow to increase with  $\text{SWC}_v$ , as found in other studies (Leo et al., 2014; Pataki et al., 2000). However, in the measurement period for this project the opposite was observed. During the study period, soil water potentials were high during the monsoon phase, when precipitation was high and  $E$  lower. Because  $E$  has a strong positive correlation with sap flow (see Figure 33) this effect overruled the effect of  $\text{SWC}_v$  resulting in the negative correlation as values were calculated on a daily base.

Because  $D$  and  $E$  both affect sap flow, a model was calculated to test if accounting for  $D$  and  $E$  would show an effect of  $\text{SWC}_v$  on sap flow. However, these models did not provide better results for any tree species. The additive models had sometimes lower significance levels for either  $E$  or  $D$  as these two variables are correlated with each other. This is often a problem when using linear models with environmental variables (Quinn et al., 2002). Ford et al. (2005) are suggesting ARIMA (autoregressive integrated moving average) models for time series modelling, especially when the included environmental variables have different cycles (i.e. irradiance – daily, soil moisture – rain events). In their study on *Pinus tadea*, ARIMA models appeared to be appropriate to model canopy transpiration based on sap flow measurements. Applying ARIMA models will be considered for future evaluations of sap flow data from the experiment.

#### 4.4 Time lags

Different parts of trees like roots, trunks, branches and leaves can store water for transpiration (Meinzer et al., 2001). When stomata open in the morning, at first the stored water is used to sustain transpiration. With a small and variable time lag, water is taken up by the roots which is measured as sap flow at the stem base. It was assumed, that the longer the time lag, the more important is the water storage (Chen et al., 2016). For estimating the water storage capacitance of trees, many studies measured the time difference between sap flow signals in the canopy and at the stem base (Köcher et al., 2013; Čermák et al., 2007; Scholz et al., 2007). In this study, the time shift between sap flow density and the environmental parameters  $D$  and  $E$  was used to represent the water storage capacitance of the studied tree species. The time shift was calculated by comparing the correlation of sap flow density and the two environmental parameters  $D$  and  $E$  while moving the time series step wise (15 minute steps). The time shift with the highest correlation for each species was used as time lag.

As  $D$  is the main physical driver of transpiration and  $E$  has a direct effect on the aperture of the stomata (Shimazaki et al., 2007; Frey et al., 2010), the trees transpiration follows changes in these two environmental parameters. When using this approach some uncertainty remains. Stomata can react differently between tree species to altered  $E$  (Woods et al., 1971) and therefore the time lags between changes in  $E$  and sap flow density also contain this effect. Results from Phillips et al. (1999) on the comparison of sap flow of different tropical trees and lianas to  $E$  and  $D$  showed, that  $E$  was the main driver of sap flow during their measurement period when looking at diurnal data. Time lags between sap flow and  $D$  were always higher than time lags of  $E$  to sap flow like in the results in this study. The authors concluded, that this time lag represents the hydraulic capacitance of the tree and that the longer time lags between sap flow and  $D$  are artefacts of the time lag already existing between  $E$  and  $D$ . As the authors also measured sap flow in the branches of the canopy, it was possible to exclude the effect of stomatal reactions. As the time lags in the branches were very small compared to the time lags measured at the tree stem base, the differences in stomatal reactions amongst the tree species only contribute little to the overall time lags. Therefore, the measured time lags in the present study are appropriate to make assumptions on the stem storage capacities of the different tree species.

In the present study, time lags differed significantly amongst tree species but not between control and treatment plots except for *Tsuga dumosa*. *Tsuga dumosa* showed the longest time lags of all species with sap flow lagging  $D$  with an average of 30 minutes and  $E$  with an average of 105 minutes. Čermák et al. (2007) found time lags in sap flow in a 57m high *Pseudotsuga menziesii* between the crown and the base of the tree between one and two hours. The diurnal increase of  $E$  generally started earlier during the day than the increase of  $D$  causing higher time lags of sap flow density with  $E$  (Figure 39).

Köcher et al. (2013) found in their study of five broadleaf trees that internal water storage was higher in diffuse porous species than in ring porous species. In their study, they evaluated time lags in sap flow between stem base and branches and also included wood anatomy and wood density measurements. In the present study, only *Quercus griffithii* is ring-porous so it was assumed that storage capacity would be low and

response to changes in  $D$  and  $E$  faster compared to other species. Although *Quercus griffithi* showed the fastest response of all species, there was no significant difference to *Quercus lanata* which has a semi-ring porous wood structure. *Quercus semecarpifolia* is also a semi-ring porous and had significantly higher time lags compared to *Quercus griffithi*. *Rhododendron arboreum* has diffuse porous wood (Dukpa et al., 2017) and similar values to *Quercus semecarpifolia*, but lower than to *Tsuga dumosa*.

Matheny et al.(2015) showed in their study of two different hardwood tree species that the ring porous species used stored water mostly during times with lower SWCv, whereas the diffuse porous species used the storage during both, wet and dry conditions. This would fit to the short time lags of *Quercus griffithi* and the sensitivity to changes in  $D$ .

#### 4.5 Sap flow and drought stress susceptibility

There are many traits that enable trees to avoid or tolerate drought (i.e. root system, stomatal behaviour, water storage capacity, carbohydrate balance) and trees adjust to drought in many ways. Sap flow is a measure to show effects on water transport and stomatal control but one has to be careful not to use only one parameter to make assumptions on the whole plant (M. G. Ryan, 2011). To assess the drought susceptibility of the species in this experiment, more data about the trees is needed.

Many studies also include leaf water potential measurements at different daytimes into the assessment of drought stress on trees (i.e. Leo et al., 2014; David et al., 2007). Although leaf water potential was measured in some trees during 2016, this was only once for the coniferous forest and twice for the broadleaf forest during the time of continuous sap flow measurements. Due to this low overlap of measurements periods, the data was not included in this study. Predawn leaf water potential measurements could provide further information about the accessibility of water for the trees and serve as an additional parameter to evaluate drought stress. Predawn water potential measurements only started in 2017 and will be included in follow up studies.

Tree ring measurements have also been done on the two experimental sites over the last years, but the data is not available yet. Comparing the different growth rates of trees with sap flow measurements may also provide deeper insights in the drought stress reactions of the species (Zang et al., 2011).

In general oaks are often identified as resistant on drought-prone sites. A study of different oak species in North America found several different strategies on how they deal with lower water availability. Deep rooting, effective water transport and xeromorphic leaves are strategies of many oak species to resist periods of drought (Abrams, 1990). Zang et al. (2011) identified oak as the most drought resistant tree species in a large comparison of tree rings of six different tree species in Southern Germany. Still, the authors put emphasis on the high intra-specific variability and that genetic differences play an important role when it comes to drought resistance of trees. When including all results from the present study, the ring porous wood structure and the smaller stem water storage capacity of *Quercus griffithi* are probably factors that are making this species more vulnerable to drought. Also a shorter leaf lifespan (deciduousness) might be a



signal of less drought resistance according to David et al. (2007) but other factors need to be considered before final conclusions can be made.

Ring porous trees seem to have a tendency to isohydric behaviour and higher probability of hydraulic failure compared to diffuse porous species. The latter tend to have more cavitation resistant vessels allowing them to keep stomata open at already very negative plant water potentials (Li et al., 2008; Taneda et al., 2008). Also in the study of Bush et al. (2008) a distinction in stomatal sensitivity to  $D$  was found between ring porous and diffuse porous trees. In the study, the authors measured higher sap flow density rates during times of low plant water potentials, caused by low  $D$ , for diffuse porous trees. This indicates a tendency to anisohydric in diffuse porous trees.

Ryan (2011) put emphasis on the importance of the carbon starvation theory for the evaluation of drought stressed trees. One example of a substantial carbon balance study in combination with a through-fall exclusion roof can be found for an experiment in the eastern Amazon rainforest (Metcalf et al., 2010). The authors were able to identify an overspending of Carbon induced by the drought caused from the throughfall exclusion roof. However, it could not be proved that the trees were starving of Carbon and if this effect would kill the trees. In contrast to the carbon starvation theory, Rowland et al. (2015) found that carbon starvation might not be responsible for tree mortality during drought in tropical forests and put more emphasis on hydraulic failure. As both studies focus on tree mortality in the tropics, the results might not be applicable to Himalayan mountain forests because of differences in the ecosystems such as climate or tree species composition (Bonal et al., 2016). This study also concludes, that both processes – hydraulic failure and carbon starvation – are synergistic responses of trees to drought but the link between the two is still not clearly understood. For the Bhutan drought stress study, data on non-structural-hydrates and hydraulic embolism are not available and these two factors could not be examined in the present study.

Combining more results from the through-fall exclusion experiment in Bhutan with sap flow data over a longer period would provide a broader base for characterizing the susceptibility of the examined tree species to drought.

#### **4.6 Conclusions and Outlook**

Most, but not all, of the tree species studied showed an effect of the rainfall exclusion on sap flow. The difference between trees on the control plots and the roof plots is for most species more pronounced in the time after the monsoon rain, which is due to higher  $D$  and  $E$  in the dry season. To study differences between control and treatment trees during the monsoon time, a longer measurement period of ideally a full year would be beneficial. Because normalised sap flux density values were partly used for the evaluation, a longer period should include some time before starting the drought experiment.

In this study, the first comparisons between the tree species hydraulic systems were possible but there was partly high variability encountered within the sap flow signals of the same tree species and treatment. This should be addressed in the future by checking the position of the sensors and the state of the sap flow

system more frequently. Also, problems with fluctuations in the power supply have to be resolved to obtain uninterrupted data.

It was possible to compare the water storage capacitance of the different tree species by calculating the time lag between sap flow and vapour pressure deficit as well as sap flow and irradiance. There were differences found in the time lag between the species which indicates the different possibilities of the trees to store water in their tissue. To estimate the storage capacitance more precisely, sap flow sensors might be mounted in the upper stem as well to have more information on the time distribution of sap flow in the trees. Shifting the sap flow signals by the time lags obtained for each tree might also yield higher correlations with irradiance and vapour pressure deficit.

The comparison of relative sap flow density with vapour pressure deficit showed a saturation effect for all tree species in times with high evaporative demand. By contrast, sap flow increased linearly with irradiance without reaching a saturation at higher irradiance levels. A comparison of relative sap flow density with volumetric soil water content did not show plausible results. This may be proved with longer time series data and the use of ARIMA models.

*Quercus griffithi* was showing traits that might make this species more susceptible to drought. The ring porous structure may make it more susceptible to hydraulic failure and also the water storage capacitance was small. However, other tree traits might be more important for the survival of this species during drought and at this point it is difficult to make conclusions on which tree species will suffer most during a monsoon failure. The inclusion of longer time series data for sap flow and additional data on the tree species like leaf water potential and growth response from tree ring analysis will provide a broader base for the evaluation of the drought susceptibility of the species studied.

## 5 Literature

- Abrams, M. D. (1990). Adaptations and responses to drought in *Quercus* species of North America. *Tree Physiology*, 7(1-2-3-4), 227–238.
- Allen, C. D., Macalady, A. K., Chenchouni, H., Bachelet, D., McDowell, N., Vennetier, M., ... Cobb, N. (2010). A global overview of drought and heat-induced tree mortality reveals emerging climate change risks for forests. *Forest Ecology and Management*, 259(4), 660–684.
- Arve, L., Torre, S., Olsen, J., & Tanino, K. (2011). Abiotic Stress in Plants - Mechanisms and Adaptations. In A. Shanker & B. Venkateswarlu (Eds.), *Abiotic Stress in Plants - Mechanisms and Adaptations* (p. 440). InTech.
- Attia, Z., Domec, J. C., Oren, R., Way, D. A., & Moshelion, M. (2015). Growth and physiological responses of isohydric and anisohydric poplars to drought. *Journal of Experimental Botany*, 66(14), 4373–4381.
- Bonal, D., Burban, B., Stahl, C., Wagner, F., Hérault, B., & Wagner, F. (2016). The response of tropical rainforests to drought — lessons from recent research and future prospects. *Annals of Forest Sciences*, 27–44.
- Bonan, G. B. (2008). Forests and climate change: forcings, feedbacks, and the climate benefits of forests. *Science*, 320(5882), 1444–1449.
- Brennicke, A., & Schopfer, P. (2010). *Pflanzenphysiologie*. Heidelberg: Spektrum Akademischer Verlag.
- Buckley, T. N. (2017). Modeling stomatal conductance. *Plant Physiology*, 174(June), 572–582.
- Busch, J., & Lösch, R. (1998). Stomatal behaviour and gas exchange of sedges (*Carex* spp.) under different soil moisture regimes. *Physics and Chemistry of the Earth*, 23(4), 443–448.
- Bush, S. E., Pataki, D. E., Hultine, K. R., West, A. G., Sperry, J. S., & Ehleringer, J. R. (2008). Wood anatomy constrains stomatal responses to atmospheric vapor pressure deficit in irrigated, urban trees. *Oecologia*, 156(1), 13–20.
- Čermák, J., Kucera, J., Bauerle, W. L., Phillips, N., & Hinckley, T. M. (2007). Tree water storage and its diurnal dynamics related to sap flow and changes in stem volume in old-growth Douglas-fir trees. *Tree Physiology*, 27(2), 181–198.
- Chen, Y. J., Bongers, F., Tomlinson, K., Fan, Z. X., Lin, H., Zhang, S. Bin, ... Zhang, J. L. (2016). Time lags between crown and basal sap flows in tropical lianas and co-occurring trees. *Tree Physiology*, 36(6), 736–747.
- Clearwater, M. J., Meinzer, F. C., Andrade, J. L., Goldstein, G., & Holbrook, N. M. (1999). Potential errors in measurement of nonuniform sap flow using heat dissipation probes. *Tree Physiology*, 19, 681–687.
- Cook, E. R., Anchukaitis, K. J., Buckley, B. M., D'Arrigo, R. D., Jacoby, G. C., & Wright, W. E. (2010). Asian monsoon failure and megadrought during the last millennium. *Science*, 328, 486–489.

- Dalsgaard, L., Mikkelsen, T. N., & Bastrup-Birk, A. (2011). Sap flow for beech (*Fagus sylvatica* L.) in a natural and a managed forest--effect of spatial heterogeneity. *Journal of Plant Ecology*, 4(1–2), 23–35.
- David, T. S., Henriques, M. O., Kurz-Besson, C., Nunes, J., Valente, F., Vaz, M., ... David, J. S. (2007). Water-use strategies in two co-occurring Mediterranean evergreen oaks: surviving the summer drought. *Tree Physiology*, 27(6), 793–803.
- Du, S., Wang, Y., Kume, T., Zhang, J., Otsuki, K., Yamanaka, N., & Liu, G. (2011). Sapflow characteristics and climatic responses in three forest species in the semiarid Loess Plateau region of China. *Agricultural and Forest Meteorology*, 151(1), 1–10.
- Dukpa, D., Katel, O., & Khandu, Y. (2017). Wood Anatomical Structure of *Rhododendron arboreum* Sm. in a Drought Manipulated Experiment under two Forest Types in Western Bhutan Himalayas. *Bhutan Journal of Natural Resources & Development*, 4(1), 1–11.
- Duursma, R. A. (2015). *Plantecophys* - An R package for analysing and modelling leaf gas exchange data. *PLoS ONE*, 10(11).
- Ford, C. R., Goranson, C. E., Mitchell, R. J., Will, R. E., & Teskey, R. O. (2005). Modeling canopy transpiration using time series analysis: A case study illustrating the effect of soil moisture deficit on *Pinus taeda*. *Agricultural and Forest Meteorology*, 130(3–4), 163–175.
- Frey, W., & Lössch, R. (2010). *Geobotanik*. Heidelberg: Spektrum Akademischer Verlag.
- Gartner, K., Nadezhidna, N., Englisch, M., Cermák, J., & Leitgeb, E. (2009). Sap flow of birch and Norway spruce during the European heat and drought in summer 2003. *Forest Ecology and Management*, 258, 590–599.
- Ghimire, C. P., Lubczynski, M. W., Bruijnzeel, L. A., & Chavarro-Rincón, D. (2014). Transpiration and canopy conductance of two contrasting forest types in the Lesser Himalaya of Central Nepal. *Agricultural and Forest Meteorology*, 197, 76–90.
- Granier, A. (1985). Une nouvelle methode pour la mesure du flux de seve brute dans le tronc des arbres. *Annales Des Sciences Forestieres*, 42(2), 193–200.
- IPCC. (2014). *Climate Change 2014: Synthesis Report. Contribution of Working Groups I, II and III to the Fifth Assessment Report of the Intergovernmental Panel on Climate Change*. (IPCC, Ed.). Geneva.
- Jentsch, A., Kreyling, J., & Beierkuhnlein, C. (2007). A new generation of events, not trends experiments. *Frontiers in Ecology and the Environment*, 5(7), 365–374.
- Khandu, Awange, J. L., & Forootan, E. (2016). An evaluation of high-resolution gridded precipitation products over Bhutan (1998-2012). *International Journal of Climatology*, 36(3), 1067–1087.
- Köcher, P., Horna, V., & Leuschner, C. (2013). Stem water storage in five coexisting temperate broad-leaved tree species: Significance, temporal dynamics and dependence on tree functional traits. *Tree Physiology*, 33(8), 817–832.
- Kück, U., & Wolff, G. (2009). *Botanisches Grundpraktikum*. Berlin, Heidelberg: Springer Berlin Heidelberg.

- Leo, M., Oberhuber, W., Schuster, R., Grams, T. E. E., Matyssek, R., & Wieser, G. (2014). Evaluating the effect of plant water availability on inner alpine coniferous trees based on sap flow measurements. *European Journal of Forest Research*, 133(4), 691–698.
- Leuzinger, S., & Körner, C. (2007). Water savings in mature deciduous forest trees under elevated CO<sub>2</sub>. *Global Change Biology*, 13(12), 2498–2508.
- Li, Y., Sperry, J. S., Taneda, H., Bush, S. E., & Hacke, U. G. (2008). Evaluation of centrifugal methods for measuring xylem cavitation in conifers, diffuse- and ring-porous angiosperms. *New Phytologist*, 177(2), 558–568.
- Lösch, R. (2001). *Wasserhaushalt der Pflanzen* (First edit). Wiebelsheim: Quelle und Meyer Verlag GmbH & Co.
- Lu, P. (2001). A direct method for estimating the average sap flux density using a modified Granier measuring system. *Functional Plant Biology*, 28(1), 85.
- Lu, P., Urban, L., & Zhou, P. (2004). Granier's Thermal Dissipation Probe (TDP) Method for Measuring Sap Flow in Trees: Theory and Practice. *Acta Botanica Sinica*, 46 (6), 631–646.
- Luis, V. C., Jimenez, M. S., Morales, D., Kucera, J., & Wieser, G. (2005). Canopy transpiration of a Canary Islands pine forest. *Agric*, 135, 117–123.
- Matheny, A. M., Bohrer, G., Garrity, S. R., Morin, T. H., Howard, C. J., & Vogel, C. S. (2015). Observations of stem water storage in trees of opposing hydraulic strategies. *Ecosphere*, 6(9), 1–13.
- McDowell, N. G., & Allen, C. D. (2015). Darcy's law predicts widespread forest mortality under climate warming. *Nature Climate Change*, 5(7), 669–672.
- McDowell, N., Pockman, W. T., Allen, C. D., Breshears, D. D., Cobb, N., Kolb, T., ... Sperry, J. (2008). Mechanisms of plant survival and mortality during drought: why do some plants survive while others succumb to drought? *New Phytologist*, 178(4), 719–739.
- Meinzer, F. C., Clearwater, M. J., & Goldstein. (2001). Water transport in trees: current perspectives, new insights and some controversies. *Environmental and Experimental Botany*, 45(3), 239–262.
- Menon, A., Levermann, A., & Schewe, J. (2013). Enhanced future variability during India's rainy season. *Geophysical Research Letters*, 40(12), 3242–3247.
- Metcalf, D. B., Meir, P., Aragão, L. E. O. C., Lobo-do-Vale, R., Galbraith, D., Fisher, R. A., ... Williams, M. (2010). Shifts in plant respiration and carbon use efficiency at a large-scale drought experiment in the eastern Amazon. *New Phytologist*, 187(3), 608–621.
- MoAF. (2017). *National Forest Inventory Report* (Vol. I).
- Nadezhdina, N., Cermák, J., & Ceulemans, R. (2002). Radial patterns of sap flow in woody stems of dominant and understory species: scaling errors associated with positioning of sensors. *Tree Physiology*, 22(13), 907–18.

- Netherer, S., Matthews, B., Katzensteiner, K., Blackwell, E., Henschke, P., Hietz, P., ... Schopf, A. (2014). Do water-limiting conditions predispose Norway spruce to bark beetle attack? *New Phytologist*, 205(3), 1128–1141.
- Om, K. (2016). Hydrological characterization of two mountain forest ecosystems in Bhutan (Master Thesis). University of Natural Resources and Life Sciences, Vienna.
- Oren, R., Sperry, J., Katul, G., Pataki, D., Ewers, B., Phillips, N., & Schäfer, K. (1999). Survey and synthesis of intra- and interspecific variation in stomatal sensitivity to vapour pressure deficit. *Plant, Cell & Environment*, 22(12), 1515–1526.
- Pallardy, S. G. (2007). The Woody Plant Body. In *Physiology of Woody Plants* (pp. 9–38).
- Pangle, R. E., Limousin, J. M., Plaut, J. A., Yepez, E. A., Hudson, P. J., Boutz, A. L., ... McDowell, N. G. (2015). Prolonged experimental drought reduces plant hydraulic conductance and transpiration and increases mortality in a piñon-juniper woodland. *Ecology and Evolution*, 5(8), 1618–1638.
- Pataki, D. E., Oren, R., & Smith, W. K. (2000). Sap flux of co-occurring species in a western subalpine forest during seasonal soil drought. *Ecology*, 81(9), 2557–2566.
- Pepin, N., Bradley, R. S., Diaz, H. F., Baraer, M., Caceres, E. B., Forsythe, N., ... Yang, D. Q. (2015). Elevation-dependent warming in mountain regions of the world. *Nature Climate Change*, 5(5), 424–430.
- Phillips, N., Oren, R., Zimmermann, R., & Wright, S. J. (1999). Temporal patterns of water flux in trees and lianas in a Panamanian moist forest. *Trees*, 14(3), 116.
- Pott, R., & Hüppe, J. (2007). *Spezielle Geobotanik*. Berlin, Heidelberg: Springer Berlin Heidelberg.
- Poudyal, K., Jha, P. K., Zobel, D. B., & Thapa, C. B. (2004). Patterns of leaf conductance and water potential of five Himalayan tree species. *Tree Physiology*, 24, 689–699.
- Quinn, G., & Keough, M. (2002). *Experimental Design and Data Analysis for Biologists* (Vol. 277). New York: Cambridge University Press.
- R Development Core Team. (2016). *R: A Language and Environment for Statistical Computing*. R Foundation for Statistical Computing Vienna Austria.
- Rowland, L., da Costa, A. C. L., Galbraith, D. R., Oliveira, R. S., Binks, O. J., Oliveira, A. A. R., ... Meir, P. (2015). Death from drought in tropical forests is triggered by hydraulics not carbon starvation. *Nature*.
- RStudio Team. (2016). *RStudio: Integrated Development for R*. Boston, MA: RStudio, Inc.,
- Ryan, J. A., & Ulrich, J. M. (2014). *xts : Extensible Time Series*. Retrieved from <http://cran.r-project.org/package=xts>.
- Ryan, M. G. (2011). Tree responses to drought. *Tree Physiology*, 31(3), 237–239.
- Schäfer, K. V. R. (2011). Canopy stomatal conductance following drought, disturbance, and death in an upland oak/pine forest of the New Jersey Pine Barrens, USA. *Frontiers in Plant Science*, 2(May), 1–7.

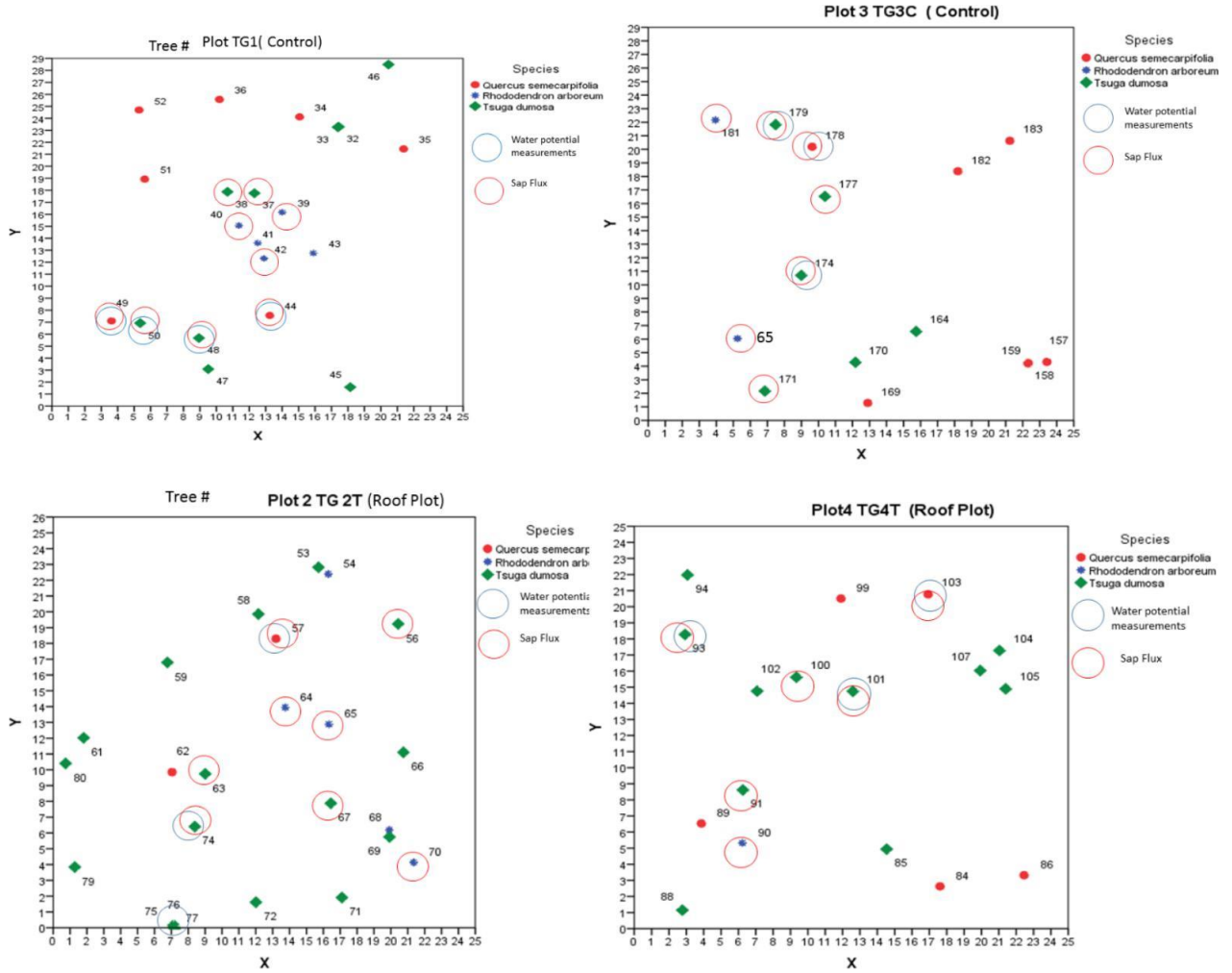
- Schewe, J., & Levermann, A. (2012). A statistically predictive model for future monsoon failure in India. *Environmental Research Letters*, 7(4), 44023.
- Schlesinger, W. H., & Jasechko, S. (2014). Transpiration in the global water cycle. *Agricultural and Forest Meteorology*, 189–190, 115–117.
- Scholz, F. G., Phillips, N. G., Bucci, S. J., Meinzer, F. C., & Goldstein, G. (2011). Hydraulic Capacitance: Biophysics and Functional Significance of Internal Water Sources in Relation to Tree Size. In F. C. Meinzer, B. Lachenbruch, & T. E. Dawson (Eds.), *Size- and Age-Related Changes in Tree Structure and Function* (pp. 341–361). Dordrecht: Springer Netherlands.
- Scholz, F. G., Bucci, S. J., Goldstein, G., Meinzer, F. C., Franco, A. C., & Miralles-Wilhelm, F. (2007). Biophysical properties and functional significance of stem water storage tissues in Neotropical savanna trees. *Plant, Cell and Environment*, 30(2), 236–248.
- Shimazaki, K., Doi, M., Assmann, S. M., & Kinoshita, T. (2007). Light Regulation of Stomatal Movement. *Annual Review of Plant Biology*, 58(1), 219–247.
- Steinkamp, J., & Hickler, T. (2015). Is drought-induced forest dieback globally increasing? *Journal of Ecology*, 103(1), 31–43.
- Taiz, L., & Zeiger, E. (2003). *Plant physiology*. Macmillan Education.
- Taneda, H., & Sperry, J. S. (2008). A case-study of water transport in co-occurring ring- versus diffuse-porous trees: contrasts in water-status, conducting capacity, cavitation and vessel refilling. *Tree Physiology*, 28(11), 1641–1651.
- Vandegehuchte, M. W., & Steppe, K. (2013). Sapflux density measurement methods: working principles and applicability. *Functional Plant Biology*, 213–223.
- Wangda, P., & Ohsawa, M. (2006a). Gradational Forest Change along the Climatically Dry Valley Slopes of Bhutan in the Midst of Humid Eastern Himalaya. *Plant Ecology*, 186(1), 109–128.
- Wangda, P., & Ohsawa, M. (2006b). Structure and regeneration dynamics of dominant tree species along altitudinal gradient in a dry valley slopes of the Bhutan Himalaya. *Forest Ecology and Management*, 230(1–3), 136–150.
- Wangdi, N. (2016). Drought stress tolerance and climate change adaption potentials of main forest types in Bhutan (PhD Thesis). University of Natural Resources and Life Sciences, Vienna.
- Wangdi, N., Mayer, M., Nirola, M. P., Zangmo, N., & Orong, K. (2017). Soil CO<sub>2</sub> efflux from two mountain forests in the eastern Himalayas, Bhutan: components and controls. *Biogeosciences*, 14, 99–110.
- Wei, T., & Simko, V. (2016). The corrplot package. Retrieved from <http://www.sthda.com>
- Woods, D. B., & Turner, N. C. (1971). Stomatal response to changing light by four tree species of varying shade tolerance. *New Phytologist*, 70(1), 77–84.
- Xu, J., & Grumbine, R. E. (2014). Building ecosystem resilience for climate change adaptation in the Asian highlands. *Wiley Interdisciplinary Reviews: Climate Change*, 5(6), 709–718.

- Xu, J., Grumbine, R. E., Shrestha, A., Eriksson, M., Yang, X., Wang, Y. U. N., & Wilkes, A. (2009). The Melting Himalayas: Cascading Effects of Climate Change on Water, Biodiversity, and Livelihoods. *Conservation Biology*, 23(3), 520–530.
- Zang, C., Rothe, A., Weis, W., & Pretzsch, H. (2011). Zur Baumarteneignung bei Klimawandel: Ableitung der Trockenstressanfälligkeit wichtiger Waldbaumarten aus Jahrringbreiten. *Allgemeine Forst- Und Jagdzeitung*, 182(5–6), 98–112.
- Zeileis, A., Grothendieck, G., Ryan, J. a, & Andrews, F. (2012). Package “ zoo .” *Cran*, 17–20.

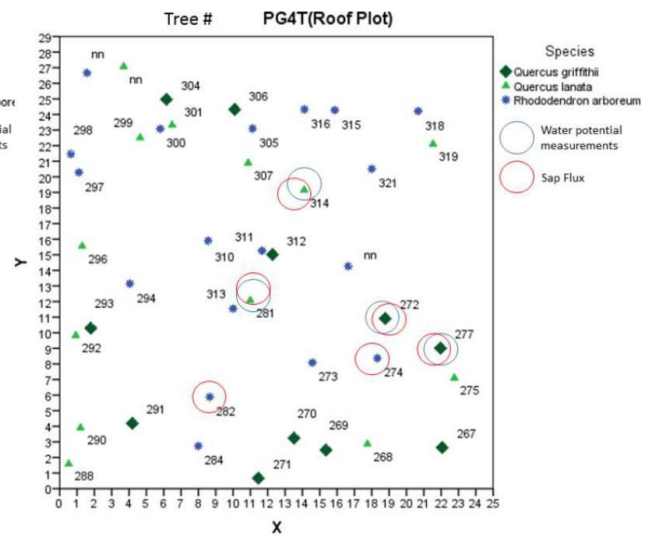
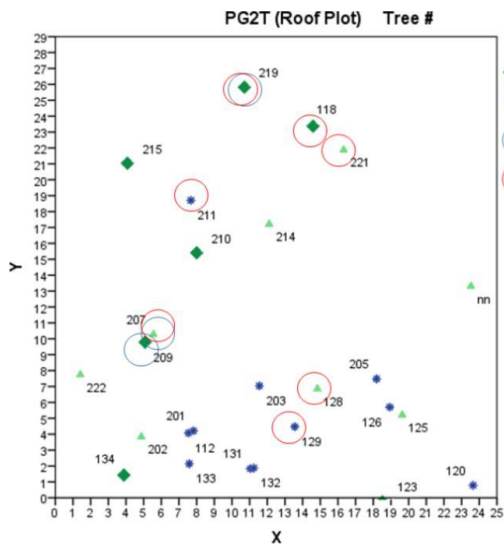
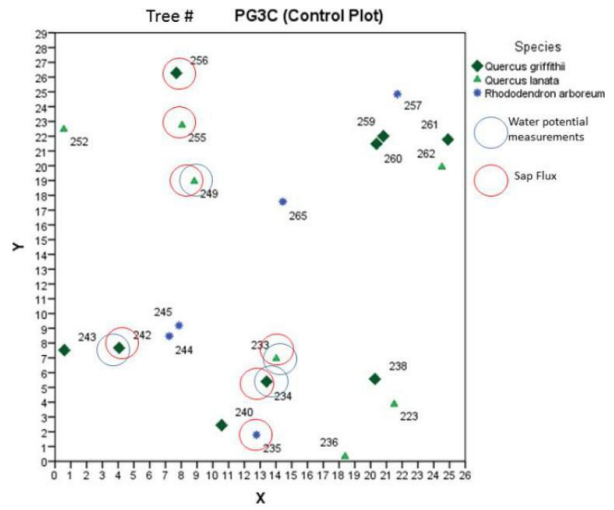
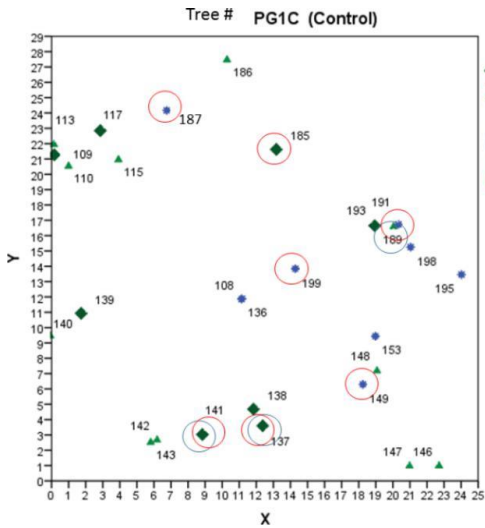


# Appendix

## A) Target trees for Sapflow and Water Potential Measurement within the experimental plots for Coniferous Site, Tashigang Goempa, Thimphu



**B) Target trees for Sapflow and Water Potential Measurement within the experimental plots for broadleaved site, Pangsho Goempa, Wmagduephodrang**



Source: Wangdi (2016)